MARTIN MARIETTA ENERGY SYSTEMS LIBRARIES
3 4456 0361355 1

83

CENTRAL RESEARCH LIBRARY
DOCUMENT COLLECTION

ORNL-2669
Physics and Mathematics

EXPERIMENTAL FORCED-CONVECTION HEAT TRANSFER WITH ADIABATIC WALLS AND INTERNAL HEAT GENERATION IN A LIQUID METAL

G. L. Muller

CENTRAL RESEARCH LIBRARY
DOCUMENT COLLECTION
LIBRARY LOAN COPY
DO NOT TRANSFER TO ANOTHER PERSON
If you wish someone else to see this document, send in name with document and the library will arrange a loan.

OAK RIDGE NATIONAL LABORATORY
operated by
UNION CARBIDE CORPORATION
for the
U.S. ATOMIC ENERGY COMMISSION

Printed in USA. Price $2.50. Available from the

Office of Technical Services
Department of Commerce
Washington 25, D.C.

LEGAL NOTICE

This report was prepared as an account of Government sponsored work. Neither the United States, nor the Commission, nor any person acting on behalf of the Commission:

A. Makes any warranty or representation, expressed or implied, with respect to the accuracy, completeness, or usefulness of the information contained in this report, or that the use of any information, apparatus, method, or process disclosed in this report may not infringe privately owned rights; or

B. Assumes any liabilities with respect to the use of, or for damages resulting from the use of any information, apparatus, method, or process disclosed in this report.

As used in the above, "person acting on behalf of the Commission" includes any employee or contractor of the Commission, or employee of such contractor, to the extent that such employee or contractor of the Commission, or employee of such contractor prepares, disseminates, or provides access to, any information pursuant to his employment or contract with the Commission, or his employment with such contractor.

ORNL-2669

Contract No. W-7405-eng-26

Reactor Projects Division

EXPERIMENTAL FORCED-CONVECTION HEAT TRANSFER WITH ADIABATIC WALLS AND INTERNAL HEAT GENERATION IN A LIQUID METAL

G. L. Muller

Submitted as a thesis to the Graduate Council of The University of Tennessee in partial fulfillment of the requirements for the degree of Master of Science.

DATE ISSUED

AUG 14 1959

OAK RIDGE NATIONAL LABORATORY
operated by
UNION CARBIDE CORPORATION
for the
U. S. ATOMIC ENERGY COMMISSION

MARTIN MARIETTA ENERGY SYSTEMS LIBRARIES

3 4456 0361355 1

ACKNOWLEDGEMENT

The author would like to express his appreciation to the following persons:

Dr. R. N. Lyon, Assistant Director of Reactor Experimental Engineering Division of the Oak Ridge National Laboratory, whose advice and interest as advisor were of great assistance.

Drs. H. F. Poppendiek and H. W. Hoffman of the Oak Ridge National Laboratory, whose support made this work possible, and whose inspiration and advice were much appreciated.

Dr. R. M. Boarts, Head of the Department of Chemical Engineering and Metallurgy, University of Tennessee, and Mr. Sylvan Cromer, Director of the Aircraft Reactor Engineering Division of the Oak Ridge National Laboratory, whose interest and support also made this work possible.

Mr. Glenn W. Greene, Mr. Jack Krewson, and members of the ARED Instrument Shop at Building 9201-3 in Y-12. The first two designed the electrical control and part of the measurement circuits and control panel.

Mr. T. N. Jones, who assisted in obtaining the data. The Y-12 craftsmen, who constructed the mercury loop.

Miss Dolores Eden, who typed this manuscript.

SUMMARY

When fluids are forced to flow through ducts, the action of viscosity causes the fluid at the walls to be stationary and to a decreasing extent retards the motion of the fluid in the flow layers outward from the wall. The internal convective heat-removal rate will thus be a function of the fluid velocity profile. If there also exists volume heat generation in the fluid with a heat evolution rate distribution which does not match the convective heat-removal distribution, temperature gradients normal to the duct walls will arise such that heat will be conducted from points in the fluid where the heat-removal rate is less than the generation rate to points where the removal is greater than the generation. To properly design systems, such as fluid-cooled nuclear reactors, wherein volume generation exists has required both analytical analyses and corroborative experiments into the effect of this interrelationship of the velocity and heat generation profiles on the over-all thermal picture.

The investigation herein reported is then an extension of the experimental and analytical work of H. F. Poppendiek[3] into the specific volume-heat-source heat-transfer problem of the flow of a liquid metal (mercury) in long, smooth, insulated pipes under internal heat generation conditions. A second aspect of this study arises in the system design whereby the adiabatic wall (by assuring that interfacial resistances will not affect the experimental results) affords a direct test of the Martinelli[11] modification for liquid metals of the heat transfer-momentum transfer analogy.

Following Poppendiek's method, analyses were obtained in detail over the liquid-metal range of Prandtl moduli for comparison with the experimental data. Then, it was found possible to rewrite the analytical expression for the heat-transfer coefficient so as to show clearly the relationship for heat transfer to fluids with and without internal heat sources. Thus, the general equation for the Nusselt modulus with volume heat generation, N_{Nu}^{*}, is:

$$\frac{1}{N_{Nu}^{*}} = 2\left[\left(1 + \frac{q_f}{q_w}\right)\int_0^1 \frac{\left[\int_0^{S_q} VSdS\right]^2}{S_q\, K_q/k}\, dS_q - \frac{q_f}{q_w}\int_0^1\int_0^{S_q}\int_0^{S_q} \frac{S_t\, V_t\, Q'''\, S}{S_q\, K_q/k}\, dS\, dS_t\, dS_q\right] \tag{1}$$

which for no heat generation reduces to Lyon's[14] integral equation for the ordinary Nusselt modulus, N_{Nu}:

$$\frac{1}{N_{Nu}} = 2\int_0^1 \frac{\left[\int_0^{S_q} VSdS\right]^2}{S_q\, K_q/k}\, dS_q \tag{2}$$

Thus, N_{Nu}^{*} is related to N_{Nu} by the expression:

$$\frac{1}{N_{Nu}^{*}} = \frac{1}{N_{Nu}} + \frac{q_f}{q_w}\, T \tag{3}$$

where T is the integral relation resulting from the substraction of equations (1) and (2).

The quantity, K_q/k, obtained from the Martinelli analogy

$$K_q/k = \left(1 + \alpha\, N_{Pr} \frac{\epsilon_m}{\nu}\right)_q \quad , \tag{4}$$

can be substituted into equations (1) and (2) to give theoretical values for the Nusselt moduli and hence T. Further, by comparison with experimental results, the analogy solution for $\alpha = 1$ as used by Poppendiek can be checked.

The experimental heat-transfer system consisted of a 1/4-in. glass tube interrupted axially by three metal electrodes through which electric current was introduced to the mercury flowing in the tube. Guard heating was employed to effect minimum heat loss through the tube wall. Thermocouples were used to measure the outside tube wall and bulk average fluid temperatures. Results were obtained over a Prandtl modulus range of 0.0191 to 0.0224 and a Reynolds modulus range of 29,000 to 164,000. It was found that the wall to mixed-mean fluid temperature differences were 49 per cent higher, on the average, than the analogy prediction. Empirically, in terms of the parameter T, the data are correlated by the equation:

$$T = \frac{1}{53 + 0.152\, N_{Pe}^{0.92}} \quad . \tag{5}$$

This was compared with theoretical predictions obtained from the approximate equations:

$$T = \frac{1}{79 + 0.226\, N_{Pe}^{0.92}} \quad , \tag{6}$$

which fits the exact solution to within ± 10 per cent for $N_{Re} \geq 10{,}000$,

or

$$T = \frac{1}{65 + 0.24\ N_{Pe}^{0.915}} \tag{7}$$

which is correct to within ± 30 per cent for $N_{Re} \geq 5{,}000$. By such comparison, it was concluded that the radial fluid molecular and/or eddy conductivity were smaller than given by analogy theories for $\alpha = 1$. This was in essential agreement with the results found in many experiments on liquid-metal heat transfer.

TABLE OF CONTENTS

CHAPTER		PAGE
I	INTRODUCTION	1
II	GENERAL THEORY OF HEAT TRANSFER WITH INTERNAL HEAT GENERATION	2
	Review and Revision of Poppendiek's Theory	2
	Calculation of Temperature Difference Parameter	9
III	EXPERIMENTAL EQUIPMENT	12
	General Considerations	12
	Equipment	13
IV	PROCEDURE	34
	System Preparation	34
	Operating Procedure	34
	Mercury-Sodium Alloy Preparation	36
	Installation of Test Sections	37
V	THE MEASUREMENTS	38
	Results	38
	Errors in the Measurements	42
	Auxiliary Measurements	43
VI	DISCUSSION	48
	Discussion of Experimental Results	48
VII	CONCLUSIONS	50
	LIST OF REFERENCES	52

TABLE OF CONTENTS (Continued)

CHAPTER PAGE

APPENDIX 54

A. Numerical Calculations of Predicted Values for T for Liquid Metals 54

B. Experimental Results and Calculations 82

C. Properties of Mercury 90

D. List of Symbols 94

LIST OF TABLES

TABLE		PAGE
I	Orifice Sizes	20
II	Positions of Thermocouple Stations	28
III	Experimental Results	39
IV	Orifice Coefficients	44
V	Values of the Function, $\frac{dq}{dA}/q''' r_w = \Phi$	57
VI	Calculation of Temperature Differences for $N_{Re} = 5000$	58
VII	Calculation of Temperature Differences for $N_{Re} = 10,000$	60
VIII	Calculation of Temperature Differences for $N_{Re} = 100,000$	62
IX	Calculation of Temperature Differences for $N_{Re} = 1,000,000$	64
X	Calculation of T for $N_{Re} = 5000$	72
XI	Calculation of T for $N_{Re} = 10,000$	73
XII	Calculation of T for $N_{Re} = 100,000$	74
XIII	Calculation of T for $N_{Re} = 1,000,000$	75
XIV	T as a Function of Reynolds' and Prandtl's Moduli	81
XV	Corrected Experimental Data	83
XVI	Corrections for Thermocouple Readings	85

LIST OF FIGURES

FIGURE		PAGE
1	Theoretical Dimensionless Wall to Mixed-Mean Fluid Temperature Differences with Insulated Wall (H. F. Poppendiek) ..	11
2	Front View of Mercury Heat-Transfer System	14
3	Side View of Mercury Heat-Transfer System	15
4	Schematic Diagram of Experimental Apparatus	16
5	Heat-Transfer Test Section	24
6	Cross Section of Exit Mixing Chamber	27
7	Electrical Power Circuit	30
8	Control Panel and Instruments	33
9	Theoretical and Experimental Differences Between Wall and Mixed-Mean Fluid Temperatures with Insulated Wall	40
10	Typical Temperatures in Test Section	41
11	Corrected Thermocouple Calibrations	46
12	Dimensionless Temperature Differences for N_{Re} = 5000 and Insulated Wall	68
13	Dimensionless Temperature Differences for N_{Re} = 10,000 and Insulated Wall	69
14	Dimensionless Temperature Differences for N_{Re} = 100,000 and Insulated Wall	70
15	Dimensionless Temperature Differences for N_{Re} = 1,000,000 and Insulated Wall	71
16	Part of Integration Graph for T for N_{Re} = 5000 and $0 \leq n \leq 0.07406$	76
17	Part of Integration Graph for T for N_{Re} = 5000 and $0.07406 \leq n \leq 1.00$	77
18	Integration Graph for T for N_{Re} = 10,000	78

LIST OF FIGURES (Continued)

FIGURE		PAGE
19	Integration Graph for T for N_{Re} = 100,000	79
20	Integration Graph for T for N_{Re} = 1,000,000	80
21	Prandtl Modulus for Mercury (Reference 14)	91
22	Properties of Mercury - Viscosity, Thermal Conductivity, Specific Heat, Electrical Resistivity (Reference 14)	92
23	Properties of Mercury - Density, Coefficient of Thermal Expansion (Reference 14)	93

CHAPTER I

INTRODUCTION

The advent of fluid-fuel-cooled nuclear reactor systems gave rise to a unique heat-transfer problem: forced-convection heat transfer with fluids containing distributed internal heat sources. Although the study of this phenomenon was originally proposed many years ago by Prandtl[1,2*] to verify his momentum-transfer theories, this area of heat transfer appears to have been neglected until the recent theoretical and analytical studies of Poppendiek.[3] Further work at the Oak Ridge National Laboratory included the problem of natural convection with internal heat generation.[4,5] Other work on volume-heated systems[6,7,8,9,10] is listed for easy reference.

This paper covers the extension to liquid metals of forced-convection heat transfer with internal heat generation. In addition to application in the area of reactor technology, the experiments described form a test of the Martinelli[11] modification of the Reynolds heat-momentum transfer analogy. This is particularly so since heat is not transferred through the channel walls; and hence, interfacial resistances such as scales or gaseous films cannot affect the heat transfer.

---

*Superscript numbers refer to similarly numbered references in the List of References at the end of the paper.

CHAPTER II

GENERAL THEORY OF HEAT TRANSFER WITH INTERNAL HEAT GENERATION

Review and Revision of Poppendiek's Theory

The theory of heat transfer in pipes carrying turbulently flowing fluids with internal heat generation was developed by H. F. Poppendiek using the modification of the heat-momentum transfer analogy of Reynolds by Martinelli. It is reviewed here since it corresponds to the conditions of the present experiments. A revision of the equations to a form similar to Lyon's integral equation[12] for the heat-transfer coefficient is made because it is somewhat easier to follow, and certain relationships are readily seen.

The conditions for the idealized system considered follow:

1. A steady state exists.
2. Temperature and velocity distributions are independent of axial position and symmetrical about the axis.
3. Constant radial heat flux at the wall.
4. Heat sources exist in the fluid and are independent of axial position and symmetrical about the axis.
5. Physical properties are not functions of temperature.
6. Physical properties are not affected by conditions of fluid flow.
7. An analogy exists between heat and momentum transfer for turbulent flow; i.e., $\epsilon_h = \alpha\, \epsilon_m$.
8. Heat is transferred by convection, molecular conduction, and eddy conduction.

It will be noted that the internal heat source need not be uniform as in Poppendiek's analysis, but only conform to condition 4.

A heat balance on an annular element of average radius, r; width, dr; and thickness, dx; gives

$$\frac{\partial}{\partial r}\left[Kr\,\frac{\partial t}{\partial r}\right] + q'''\,r = \gamma\, c_p\,\frac{\partial t}{\partial x}\,ru \tag{8}$$

Downstream from the entrance, where the thermal boundary layers are established, the axial temperature gradient is constant. Its value is found from a heat balance on a stationary differential lattice. Integrating equation (8), we have:

$$kr_w\left(\frac{dt}{dr}\right)_w + \int_o^{r_w} q'''\,r\,dr = \gamma\, c_p\,\frac{d}{dx}\int_o^{r_w} tur\,dr \tag{9}$$

Let $\frac{dq}{dA} = -\,K\,\frac{dt}{dy}$, where y is the distance from the pipe wall or $r_w - r$; then, $\frac{dq}{dA} = K\,\frac{dt}{dr}$; and at the pipe wall, K = k; so that $\left(\frac{dq}{dA}\right)_w = k\,\left(\frac{dt}{dr}\right)_w$.

Now,

$$t_m = \frac{\int_o^{r_w} \gamma\, c_p\, tur\, 2\pi\, dr}{\int_o^{r_w} \gamma\, c_p\, ur\, 2\pi\, dr} = \frac{2}{u_m\, r_w^2}\int_o^{r_w} tur\,dr\ ^{*} \tag{10}$$

and, similarly,

$$q_m''' = \frac{\int_o^{r_w} q'''\,r\,dr}{\int_o^{r_w} r\,dr} = \frac{2}{r_w^2}\int_o^{r_w} q'''\,r\,dr \tag{11}$$

---

*This is known as the mixed-mean or bulk-average fluid temperature and is not a simple temperature average, but results from the average thermal energy content in the fluid flowing past a given axial position.

Substituting equations (10) and (11) into equation (9) gives:

$$\frac{1}{r_w}\left(\frac{dq}{dA}\right)_w + \frac{q_m'''}{2} = \gamma\, c_p \frac{\partial t_m}{\partial x}\,\frac{u_m}{2}$$

Thus,

$$\frac{\partial t_m}{\partial x} = \frac{\frac{2}{r_w}\left(\frac{dq}{dA}\right)_w + q_m'''}{\gamma\, c_p\, u_m} = \frac{\partial t}{\partial x} \tag{12}$$

since the temperature distribution is independent of axial position. Thus, the following total differential equation is obtained:

$$\frac{d}{dr}\left[Kr\,\frac{dt}{dr}\right] + q'''\,r = \left[\frac{2}{r_w}\left(\frac{dq}{dA}\right)_w + q_m'''\right]\frac{u}{u_m}\,r \tag{13}$$

Performing the integration between $r = 0$ and $r = r_q$, we have

$$Kr_q\,\frac{dt}{dr_q} + \int_0^{r_q} q'''\,rdr = \frac{\left[\frac{2}{r_w}\left(\frac{dq}{dA}\right)_w + q_m'''\right]}{u_m}\int_0^{r_q} urdr$$

or,

$$\frac{dt}{dr_q} = \left[\frac{\frac{2}{r_w}\left(\frac{dq}{dA}\right)_w + q_m'''}{u_m\, r_q\, K}\right]\int_0^{r_q} urdr - \frac{\int_0^{r_q} q'''\,rdr}{r_q\, K} \tag{14}$$

Again, integrating from $r_q = r_t$ to $r_q = r_w$ gives

$$t_w - t = \left[\frac{2}{r_w}\left(\frac{dq}{dA}\right)_w + q_m'''\right]\int_{r_t}^{r_w} \frac{\int_0^{r_q} \frac{u}{u_m}\,rdr}{r_q\, K}\,dr_q$$

$$- q_m'''\int_{r_t}^{r_w} \frac{\int_0^{r_q} \frac{q'''}{q_m'''}\,rdr}{r_q\, K}\,dr_q \tag{15}$$

Using the foregoing definition for t_m,

$$t_w - t_m = \frac{\int_o^{r_w} (t_w - t)\, r_t\, u dr_t}{\int_o^{r_w} r_t\, u dr_t} = \frac{2}{r_w^2\, u_m} \int_o^{r_w} (t_w - t)\, r_t\, u dr_t \qquad (16)$$

Substituting equation (15) into equation (16), and changing the integration variable, it follows that

$$t_w - t_m = 2\int_o^1 \frac{r_t}{r_w}\, \frac{u}{u_m} \left\{ \left[2r_w \left(\frac{dq}{dA}\right)_w \right.\right.$$

$$\left. + q_m''' r_w^2 \right] \int_{\frac{r_t}{r_w}}^1 \frac{\int_o^{\frac{r_q}{r_w}} \frac{u}{u_m} \frac{r}{r_w}\, d\left(\frac{r}{r_w}\right)}{\frac{r_q}{r_w} K}\, d\left(\frac{r_q}{r_w}\right) \qquad (17)$$

$$\left. - q_m''' r_w^2 \int_{\frac{r_t}{r_w}}^1 \frac{\int_o^{\frac{r_q}{r_w}} \frac{q'''}{q_m'''} \frac{r}{r_w}\, d\left(\frac{r}{r_w}\right)}{\frac{r_q}{r_w} K}\, d\left(\frac{r_q}{r_w}\right) \right\} d\left(\frac{r_t}{r_w}\right)$$

Making the substitutions $S = \frac{r}{r_w}$, $V = \frac{u}{u_m}$, $Q''' = \frac{q'''}{q_m'''}$ there is obtained

$$t_w - t_m = 2\int_o^1 S_t\, V_t \left\{ \left[2r_w \left(\frac{dq}{dA}\right)_w \right.\right.$$

$$\left. + q_m''' r_w^2 \right] \int_{S_t}^1 \frac{\int_o^{S_q} VS\, dS}{S_q\, K}\, dS_q \qquad (18)$$

$$\left. - q_m''' r_w^2 \int_{S_t}^1 \frac{\int_o^{S_q} Q'''\, SdS}{S_q\, K}\, dS_q \right\} dS_t$$

Rearranging terms and dividing through by the thermal conductivity, k, results in the following equation:

$$t_w - t_m = 2\,\frac{q_m''' \; r_w^2}{k} \int_o^1 \int_{S_t}^1 \int_o^{S_q} \frac{S_t \; V_t \; (VS - Q''' \; S)}{S_q \; K/k} \, dS \; dS_q \; dS_t$$

$$+ \frac{4r_w}{k} \left(\frac{dq}{dA}\right)_w \int_o^1 \int_{S_t}^1 \int_o^{S_q} \frac{S_t \; V_t \; VS}{S_q \; K/k} \, dS \; dS_q \; dS_t \tag{19}$$

The order of the integrals can be changed by appropriate changes in the limits. Thus, the equation may be written

$$t_w - t_m = 2\,\frac{q_m''' \; r_w^2}{k} \int_o^1 \int_o^{S_q} \int_o^{S_q} \frac{S_t \; V_t \; (VS - Q''' \; S)}{S_q \; K/k} \, dS \; dS_t \; dS_q$$

$$+ \frac{4r_w}{k} \left(\frac{dq}{dA}\right)_w \int_o^1 \int_o^{S_q} \int_o^{S_q} \frac{S_t \; V_t \; VS}{S_q \; K/k} \, dS \; dS_t \; dS_q \tag{20}$$

which is the same as the following equation, since S is independent of S_t.

$$t_w - t_m = 2\,\frac{q_m''' \; r_w^2}{k} \int_o^1 \frac{\left[\int_o^{S_q} VSdS\right]^2}{S_q \; K/k} \, dS_q$$

$$- 2\,\frac{q_m''' \; r_w^2}{k} \int_o^1 \int_o^{S_q} \int_o^{S_q} \frac{S_t \; V_t \; Q''' \; S}{S_q \; K/k} \, dS \; dS_t \; dS_q \tag{21}$$

$$+ \frac{4r_w}{k} \left(\frac{dq}{dA}\right)_w \int_o^1 \frac{\left[\int_o^{S_q} VSdS\right]^2}{S_q \; K/k} \, dS_q$$

It is seen that the temperature differences caused by the internal heat generation are directly additive to those caused by ordinary heat transfer,

since with no internal heat generation, equation (21) reduces to the last term (Lyon's[12] integral equation for the Nusselt modulus):

$$\frac{k(t_w - t_m)}{2r_w \left(\frac{dq}{dA}\right)_w} = \frac{1}{N_{Nu}} = 2 \int_o^1 \frac{\left[\int_o^{S_q} VSdS\right]^2}{S_q \; K/k} \, dS_q \tag{22}$$

If internal heat generation exists, and there is no wall heat flow, equation (21) reduces to

$$\frac{k(t_w - t_m)}{q_m''' \; r_w^2} = T = 2 \left\{ \int_o^1 \frac{\left[\int_o^{S_q} VSdS\right]^2}{S_q \; K/k} \, dS_q - \int_o^1 \int_o^{S_q} \int_o^{S_q} \frac{S_t \; V_t \; Q''' \; S}{S_q \; K/k} \, dS \, dS_t \, dS_q \right\} \tag{23}$$

or

$$T = 2 \int_o^1 \int_o^{S_q} \int_o^{S_q} \frac{S_t \; V_t \; (V - Q''') \; S}{S_q \; K/k} \, dS \, dS_t \, dS_q \tag{24}$$

For a case where the velocity distribution exactly matches the internal heat generation distribution, such as slug flow and uniform internal heat generation,

$$T = 0$$

For uniform internal heat generation and no wall heat flow - the case which was studied here - equation (23) reduces to

$$T = 2 \left\{ \int_o^1 \frac{\left[\int_o^{S_q} VSdS\right]^2}{S_q \; K/k} \, dS_q - \int_o^1 S_q \frac{\int_o^{S_q} V_t \; S_t \; dS_t}{K/k} \, dS_q \right\} \tag{25}$$

Getting back to the general case, since the wall heat transfer is uniform,

$$\left(\frac{dq}{dA}\right)_w = \frac{q_w}{A_w} = \frac{q_w}{2\pi r_w (x_2 - x_1)} \quad ;$$

and since the internal generation is independent of axial distance,

$$q_f = q_m''' \pi r_w^2 (x_2 - x_1) \quad ,$$

equation (21) can then be written as

$$\frac{1}{N_{Nu}^*} = 2 \left\{ \left[\frac{q_f}{q_w} + 1 \right] \int_0^1 \frac{\left[\int_0^{S_q} VSdS \right]^2}{S_q \, K/k} \, dS_q \right. \tag{26}$$

$$\left. - \frac{q_f}{q_w} \int_0^1 \int_0^{S_q} \int_0^{S_q} \frac{S_t \, V_t \, Q''' S}{S_q \, K/k} \, dS \, dS_t \, dS_q \right\}$$

It is thus seen that N_{Nu}^* is related to the ordinary Nusselt modulus by:

$$\frac{1}{N_{Nu}^*} = \frac{1}{N_{Nu}} + \frac{q_f}{q_w} T \tag{27}$$

It is observed that the presence of internal heat generation raises the apparent Nusselt modulus for wall cooling, and decreases it for heating.

Consider that $q_f = q_w$. Thus, since

$$q_f = q_m''' \pi r_w^2 \ell \quad , \tag{28}$$

and

$$q_w = \left(\frac{dq}{dA}\right)_w 2\pi r_w \ell \quad , \tag{29}$$

then

$$q''' r_w = 2 \left(\frac{dq}{dA}\right)_w \tag{30}$$

Now, by definition,

$$\frac{1}{N_{Nu}} = \frac{k\,(t_w - t_m)}{\left(\frac{dq}{dA}\right)_w 2r_w} \tag{31}$$

and

$$T = \frac{k\,(t_w - t_m)}{q_m''' \; r_w^2} \tag{32}$$

Since all terms on the right-hand sides of equations (31) and (32) are equal exept $(t_w - t_m)$ and since T is much smaller than $\frac{1}{N_{Nu}}$ for a given Peclet number, it follows that for a much smaller wall to mixed-mean fluid Δt than with ordinary heat transfer the same amount of heat can be added by generating it internally in the fluid. The reason, of course, is that the heat is generated uniformly in the fluid and only a small part of it must traverse the high-resistance region near the wall, whereas almost all of the heat added externally must go through this region.

Equation (27), when applied to Stromquist's experiments[13] for the given condition that 6 per cent of the heat generated in the test section was generated in the mercury, shows (using measured values of N_{Nu} and T) that the Nusselt modulus decreases by only approximately 0.5 per cent. This is negligible as compared with the errors incurred in the measurements.

Calculation of Temperature Difference Parameter

Calculations were made of the temperature differences occurring in fluids flowing turbulently through pipes having Prandtl moduli of 0.002, 0.005, 0.02, 0.05, and 0.10 following the numberical calculation procedures outlined by Poppendiek in his paper.[3] This was done to provide more complete coverage of the liquid-metal Prandtl moduli so as to

afford a theoretical comparison for the experimental results. The results of the calculations are shown in Fig. 1 along with Poppendiek's results. Details of the calculations are in the Appendix.

It was found that the approximate equation:

$$T = \frac{1}{79 + 0.226\ N_{Pe}^{0.92}} \tag{33}$$

fits the liquid-metal predictions within ± 10 per cent for $N_{Re} \geqq 10{,}000$ and $0 \leq N_{Pr} \leq 0.10$.

A second equation:

$$T = \frac{1}{65 + 0.24\ N_{Pe}^{0.915}} \tag{34}$$

fits the predictions within ± 30 per cent for $N_{Re} = 5{,}000$ and $0 \leq N_{Pr} \leq 0.10$.

The experiment, which will be described in the following chapter, was thus designed to fulfill the conditions set forth here, namely:

a. Forced convection in a straight circular pipe of sufficient length to avoid end effects.

b. A low Prandtl-modulus fluid, i.e., mercury.

c. Uniform internal heat generation in the mercury.

d. No wall heat transfer (insulated walls).

e. A wide range of flow rates (Reynolds moduli).

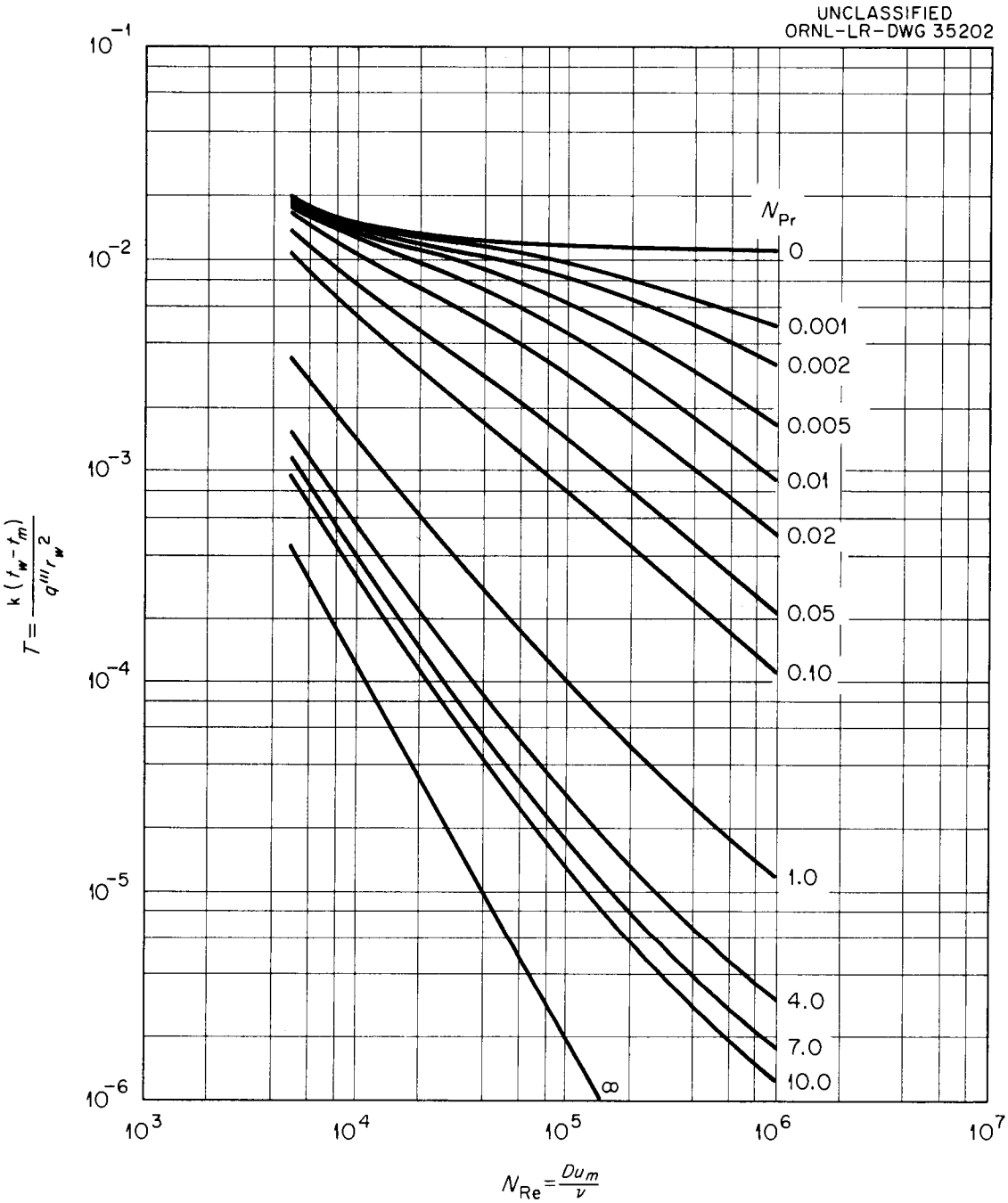

Fig. 1. Theoretical Dimensionless Wall to Mixed-Mean Fluid Temperature Differences with Insulated Wall.

CHAPTER III

EXPERIMENTAL EQUIPMENT

General Considerations

The liquid metal chosen for the experiment was mercury, because its low melting point (-38°F) obviated the need for complicated auxiliary heating equipment. The method chosen for generating the internal heat source in the fluid was direct electrical resistance heating because of the relative simplicity and the uniform heat source that it afforded. Another possible scheme was electrical induction heating.

The test section was arranged so that the flow was vertically upward. In this manner, any trapped gas would be swept out of the test section during operation.

To insure that the wall heat transfer would be kept to a minimum, the test section was insulated and automatically controlled guard heaters maintained the insulation outside diameter temperature at the tube wall temperature.

A positive-displacement screw-type pump was chosen over centrifugal types because much less air would be entrained in the mercury due to the pumping action.

Quarter-in.-ID glass tubes were chosen for the test section with an over-all length-to-diameter ratio of 70 to insure fully developed thermal boundary layers. Included in the test-section length were three electrodes by which current was conducted to the mercury. A 210-diameter length of 1/4-in.-ID tubing preceded the test section as a calming length.

The mixed-mean fluid temperatures were measured, the inlet temperature by means of wall thermocouples on the calming length which was insulated and always operated near room temperature and the exit temperature by a mixing chamber filled with baffles followed by a thermocouple in a well.

The wall temperatures were measured on the outside of the glass tubes with thermocouples, and corrections based on the Δt between the insulation outside diameter and the outside tube wall were made to obtain the glass-mercury interface temperature.

Due to the physiological hazards associated with mercury, the system was located in Building 9201-2, Y-12 Plant, Oak Ridge, Tennessee, which was equipped for handling mercury. The location was well ventilated, and a concrete basin with a drain leading to a catch tank on the floor below served to contain any spilled mercury. The principal leak locations were the Swagelok and screwed fittings used with tubing connecting the orifices and differential pressure cells, and the pump packing, which leaked occasionally. Respirators were worn during transfers of mercury to and from the system. The system itself was completely enclosed. Safety checks were made with a General Electric mercury vapor detector.

Equipment

Flow Circuit

Front and side views of the experimental equipment are shown in Figs. 2 and 3, respectively. Fig. 4 is a schematic diagram of the flow circuit. Mercury was circulated by the pump from the sump through a surge tank, any of the flow measurement orifices, the test section, the main

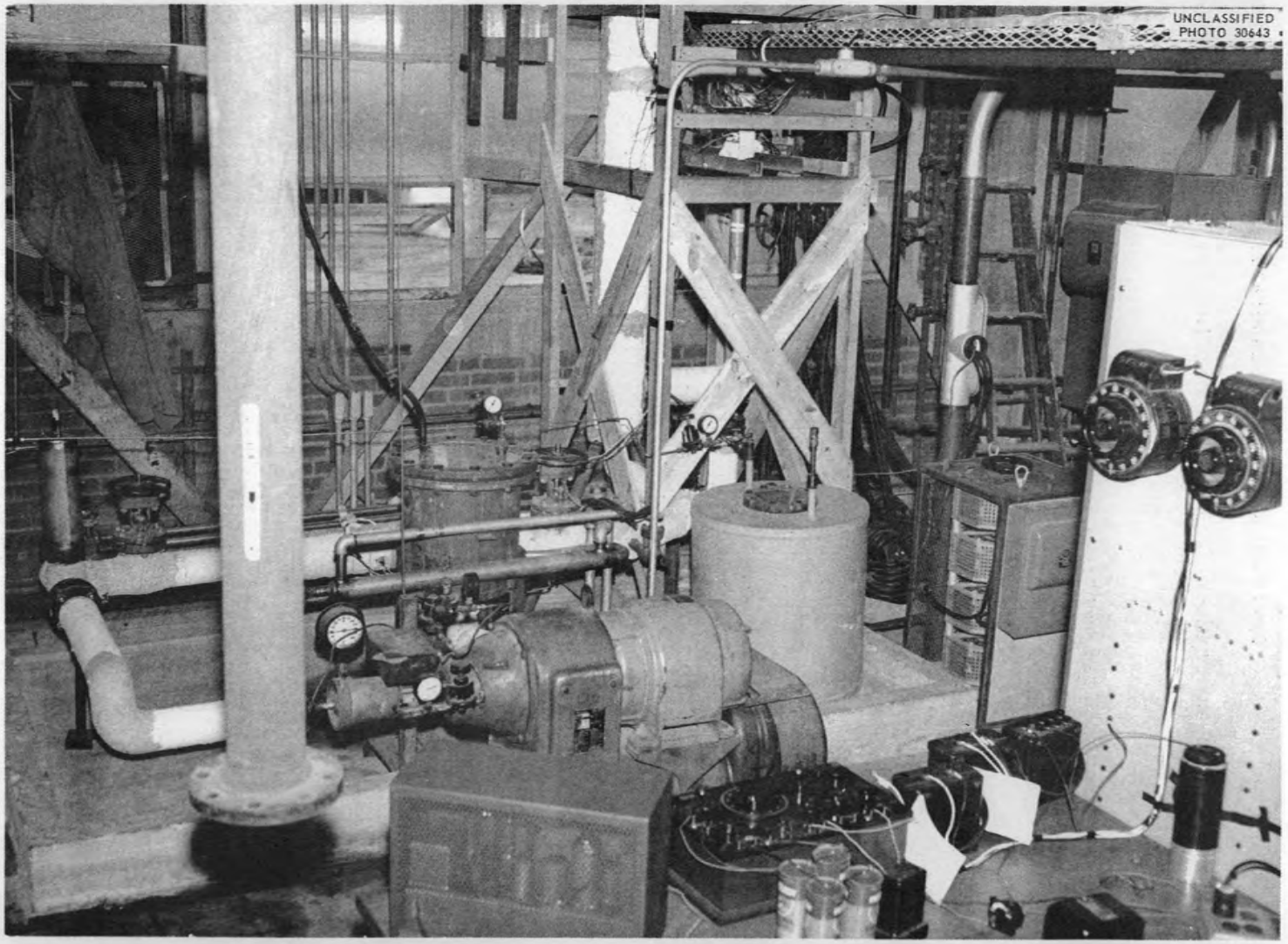

Fig. 2. Front View of Mercury Heat-Transfer System.

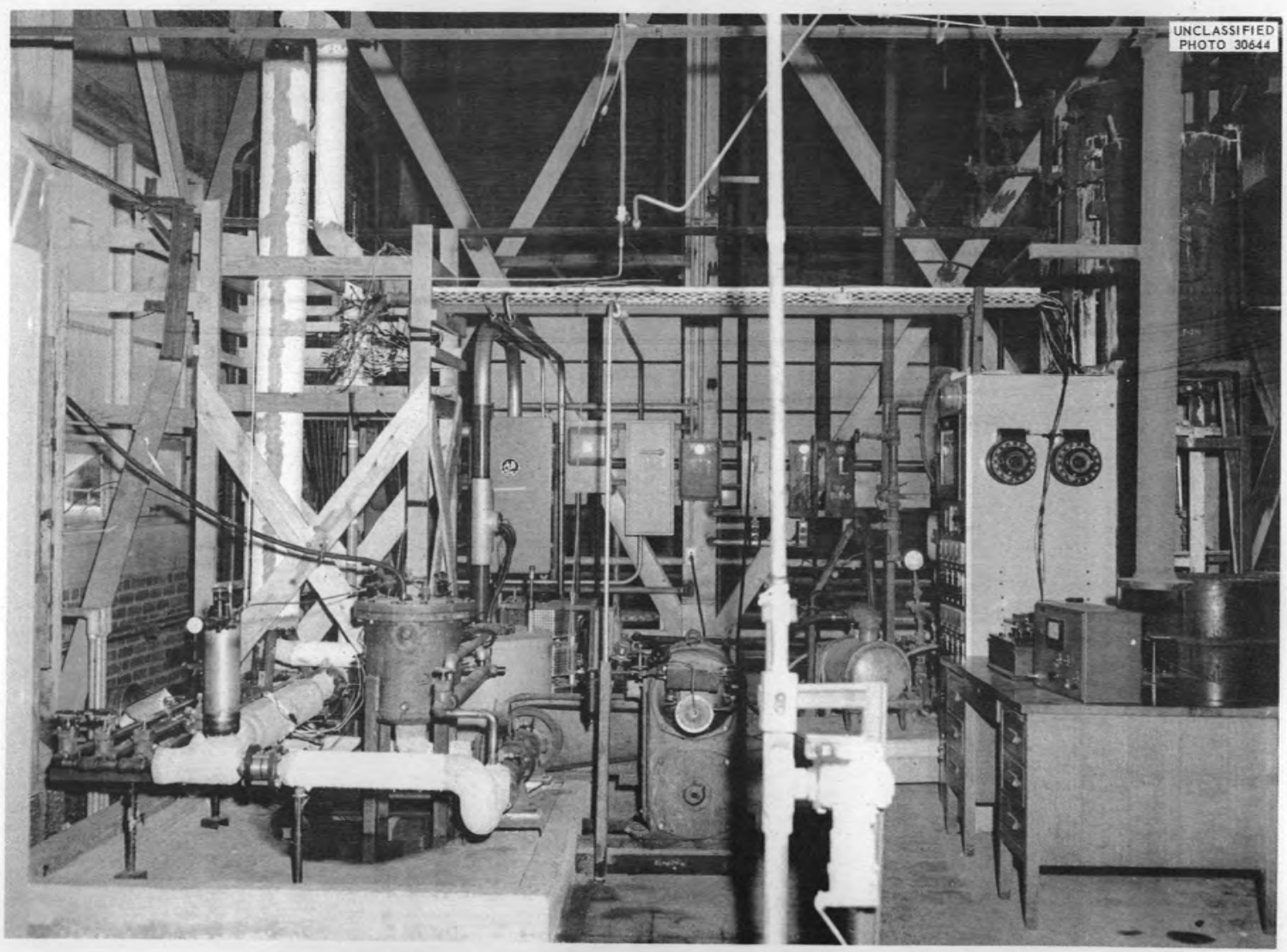

Fig. 3. Side View of Mercury Heat-Transfer System.

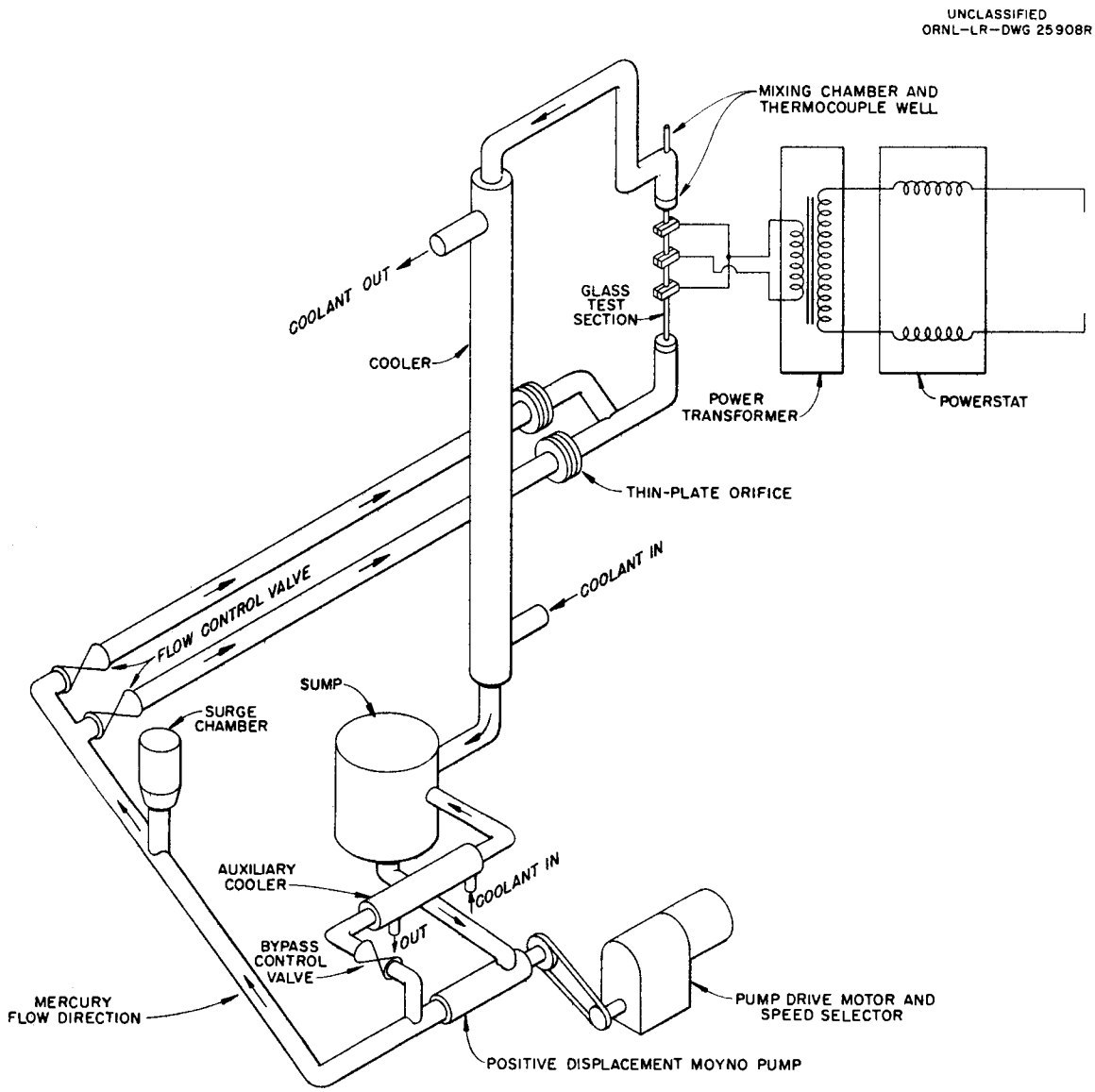

Fig. 4. Schematic Diagram of Experimental Apparatus.

heat exchanger, and back to the sump. An auxiliary circuit equipped with a small heat exchanger bypassed the test section. The flow control valves were used for orifice selection as well as flow rate control. The bypass control valve served to regulate the pump output pressure to any desired value. A cutoff valve on the return line to the sump served to route the flow through an exit valve which was connected by a rubber hose to a small enclosed tank on a scale. This arrangement was used when the orifice calibrations were made. A storage tank was connected to the pump intake pipe by a short length of piping an a cutoff valve.

Materials of Construction

Mild steel and 316 and 347 stainless steels were the metals used in contact with mercury. Pyrex glass was used for the test-section tube. Neoprene rubber was used in gaskets and the pump stator. The stainless steels were preferred because of their rust-resistant properties. However, stainless ells, tees, reducers, and flanges were not available and mild steel was substituted. Galvanized and steel piping was used for the coolant water.

Pump

The pump employed was a Robbins and Myers 1L6-frame "Moyno". It was a positive-displacement screw-type pump having a rubber stator and a steel rotor. Its capacity was 5.02 gal/100 rpm and 200 lb/in.^{2} at 370 rpm and no flow. It worked satisfactorily for a time and then began to bind and stick about halfway through the tests. Since the pump depended upon the mercury for lubrication between the rotor and stator, the cause of the

sticking was evident. Since it was known that small amounts of sodium added to mercury allowed wetting of steel surfaces,[13] enough sodium to make an alloy of Hg-0.02 w/o Na was added to the system. Upon addition, the pump immediately began operating normally, indicating that it was being lubricated. No further pump trouble was encountered. The small amount of sodium added was not sufficient to appreciably affect the thermal and electrical properties.

Mercury leakage occurred at the packing occasionally, but was easily corrected and was not serious.

Piping

Welded joints, tested for cracks with penetrating dye, were used wherever possible. Where it was necessary to disconnect parts of the system, 150-lb flanged joints were used having 3/16-in.-thick Neoprene rubber gaskets. One-in. and two-in. stainless piping was used. Tees, ells, and reducers were of mild steel. Stainless 1/4-in. tubing and Swagelok fittings were used in the orifice pressure measurement system. The entire system was leak checked under vacuum with a helium leak detector. Several leaks were found; mainly in the Swagelok fittings, in two welds which had not been previously dye checked, and the pump gaskets. These were subsequently remedied. The piping was essentially leak free during operation with mercury except for some screwed fittings and Swagelok fittings on the orifice tubing.

Valves

Fulton Sylphon bellows-sealed 347 stainless steel globe valves were used in 1-in. and 2-in. sizes. The valves had welding fittings and, without exception, gave trouble-free service. One-fourth-in. needle valves with Swagelok fittings were used as shutoff valves for the orifice measurement system, and two were used in parallel with two 1-in. control valves to achieve better flow control. The valves developed small leaks about the stems and Swagelok fittings occasionally. Most of these were easily corrected by tightening the stem and Swagelok nuts.

Flowmeters

Thin-plate VDI-type orifices were used as flowmeters. To accommodate a wide range of flow rates and for ease of operation, four orifices sized so as to complement each other were connected in parallel, each with its separate control valve and run. The sizes are listed in Table I.

Flange taps were used; however, the piping was welded to the outside of the slip-on flange, instead of being pushed through the flange and welded at the flange face. This arrangement undoubtedly would affect the orifice pressure drop, since the flow area immediately before and after the orifice plate was larger than the pipe area, and because the pressure taps were located in this region.

The orifice pressure drop was measured by either of two Swartout differential pressure cells. Movement of a diaphragm in the cells by a pressure differential imposed by the orifice pressure drop induced a voltage in a differential transformer. The signal was recorded on a strip-chart

TABLE I

ORIFICE SIZES

Orifice	Orifice Diameter (in.)	Pipe Diameter (in.)
1	0.081	1.049
2	0.255	1.049
3	0.741	1.049
4	1.441	2.067

recorder. The system mercury was used to transmit the pressure to the cell diaphragm. Any of the orifices could be connected to either of the cells by manipulating the proper cutoff valves.

The cells had ranges of 0-20 and 0-200 in. of water, respectively, to complement each other. The measurement system accuracy was 1/2 per cent of the full-scale reading. However, the cells were subject to zero-shifting if a pressure differential greater than the range of measurement was imposed.

Calibration and operation of the flowmeter will be described in the procedure.

Heat Dumps

The main and auxiliary heat exchangers served to dispose of heat generated in the mercury system to coolant water supplied from the building system.

The main cooler was a cross-baffled shell-and-tube arrangement. The mercury flowed through a single pass of 37 3/8-in. tubes, each 8 ft long and spaced on 9/16-in. centers in a delta array. The coolant water passed between the tubes inside an outer shell of 4-in. pipe. Baffles forced the water to flow in a sinuous fashion, back and forth across the tubes. The cooler was designed to transfer 100 kw of heat at a mercury flow rate of 26.5 gal/min. This would cool the mercury to 80°F using water at 70°F.

The auxiliary cooler was a concentric-tube exchanger formed by a 1-in. pipe and a 2-in. pipe. It was 30 in. long. Water flowed in the shell counter to the mercury flow direction. The cooler formed part of

the bypass circuit.

Storage Tank

A tank for mercury storage was made of a 2-ft length of 24-in. steel pipe with 1-in.-thick plates welded on each end. A boiler gauge welded to the side of the tank was used for mercury level indication. A 5-in.-dia hand hole in the top plate, with a bolted 1-in.-thick Plexiglas cover, afforded access to the tank. A pipe connection at the top allowed the tank to be pressurized or vented. A second pipe extended through the top to the floor of the tank. The tank was filled through this pipe, and could be emptied through it by pressurizing the tank. A third pipe at the floor level of the tank formed a connection with the pump intake line, and was equipped with a cutoff valve. The mercury in the tank could be pressured into the system, and drained from the system into the tank by a combination of gravity, pressurization of the sump, and reversal of the pump to remove the mercury trapped in the pump output piping.

Sump Tank

The sump was made of 1/2-in.-thick stainless steel, 15 in. in inside diameter and 18 in. deep, including the ellipsoidal bottom. To the top flange was bolted a 1-in.-thick Plexiglas plate with a rubber gasket. The tank could be pressurized through a pipe connection at the top. A second pipe connection could be used for venting through a rubber hose led outside the building and was equipped with a pinch clamp. It was sometimes used for filling the tank. Two lines led into the tank

from the main and auxiliary circuits. The openings were below the normal level of mercury in the tank, and the incoming streams struck a baffle placed in front of the openings. The pump intake line was connected to the bottom of the tank, and a second baffle prevented vortices from forming.

Surge Chamber

The surge chamber was a 12-in. length of 4-in. pipe connected by a 4 x 2-in. reducer to the main circuit piping between the control valves and the pump output. Two spark plug probes were used to obtain a rough idea of the mercury level in the chamber. A tube connection to the top served to pressurize and vent the chamber. The chamber served to reduce any pulsations induced by the pump. It was found that the chamber worked well with the air initially trapped there. Pulsations of flow could not be detected on the orifice pressure drop recorder even though pressure pulsations of approximately ± 10 per cent maximum at the pump output were detectable with a 600-lb stainless steel Bourdon-tube gauge.

The Test Section

The heat-transfer test section, shown in Fig. 5, consisted of a 0.250-in.-ID tube 47-13/16 in. long. This length was made up of a 30-in. calming length of stainless steel tubing followed by a 1-1/2-in. long steel electrode, a 6-5/8-in. length of precision-bored glass tubing, a second electrode, a second 6-11/16-in. long precision-bored glass tube, and a third electrode.

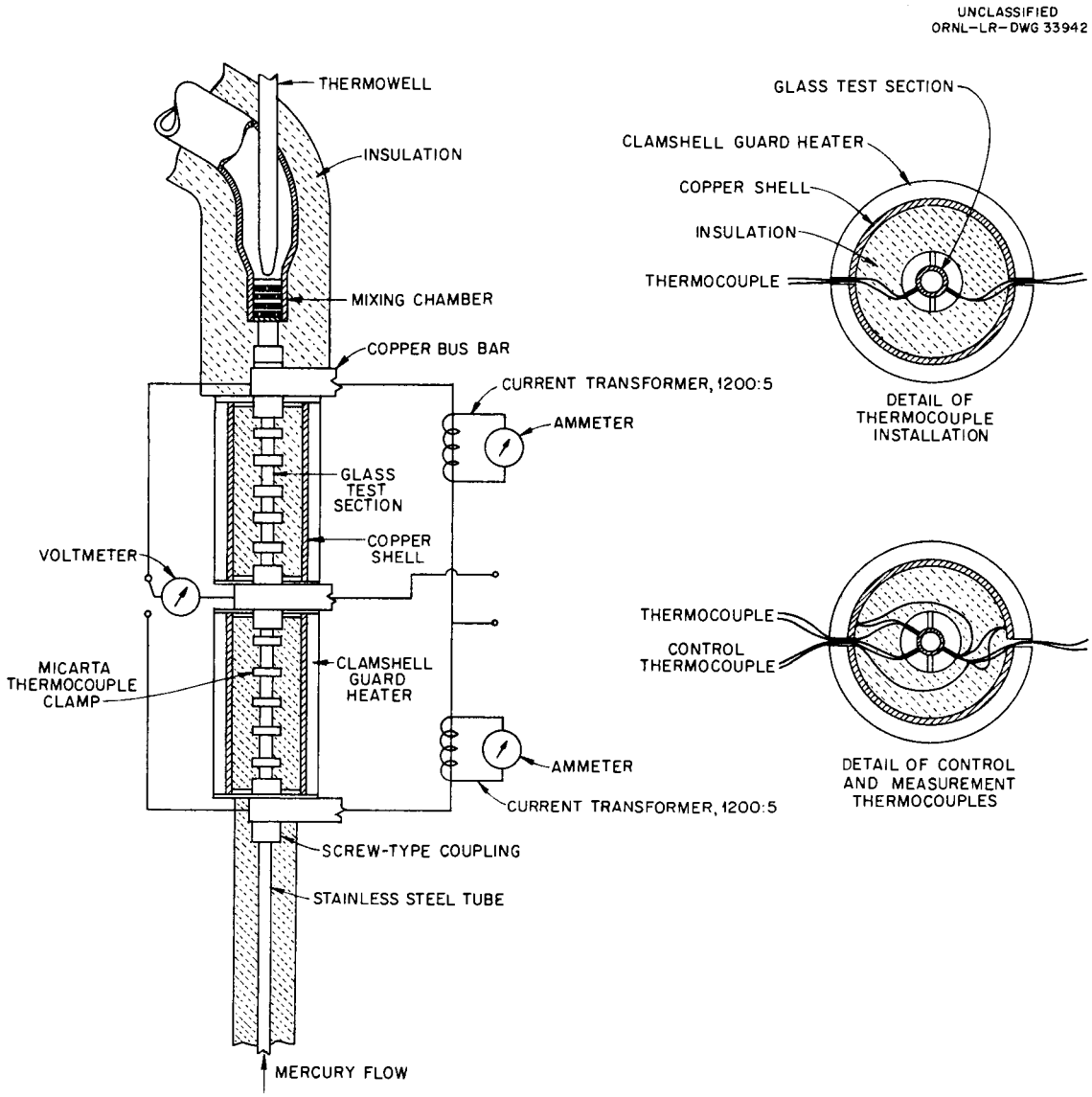

Fig. 5. Heat-Transfer Test Section.

Considerable trouble was encountered in the test-section installation due to breakage of the glass test sections. The massive bus bar connections relative to the thin (1/16-in.-thick wall) glass tubes, and thermal expansions contributed to the breakage. However, these troubles were overcome by careful handling and the methods outlined in the chapter on procedure. No trouble of any kind was subsequently encountered with the test section during thermocouple installation or operation at pressures up to 150 lb/in.^{2}

The electrodes had small, 0.020-in. high lips extending above the gasket sealing faces so that the gap between electrode and glass tubing was reduced to a minimum when the couplings were tightened, thus affording a smooth transition for the mercury flow. The bus bars and test-section assembly were supported by a framework of wood 2 x 4's. The bus bars consisted of three 1 x 3/8-in. copper bars which were bolted together and to the electrode assemblies. The contact areas were silvered to assure good conduction.

The test section was insulated by a Fiberglas "cotton" packed into 1/8-in.-thick copper cylinders 3 in. in outside diameter. The cylinders were split in half lengthwise, and covered the area between the electrodes. Clamshell heaters were placed around the copper cylinders as guard heaters. Six separately controlled heaters were spaced along the length of the test section. Insulation was used around the inlet calming length and the exit mixing chamber.

Temperature Measurements

To obtain exit bulk fluid temperatures, the mixing chamber shown in Fig. 6 was used consisting of four "disk-and-doughnut" baffles in a 1-in. diameter by 1-1/2-in. long shell followed by a thermowell. A 36-gauge copper-constantan thermocouple was placed in the thermowell so that it contacted the sealed end.

No. 36-gauge copper-constantan thermocouples were clamped to the outside of the glass tubing by Micarta clamps with a groove cut in the clamping face to hold the thermocouple junction in position. The leads were led out in a plane normal to the tube axis, first along the circumference of the tube for 1/8 in. and then radially outward through a hole drilled in the Micarta clamp. In this manner, the leads near the junction were kept in an isothermal region. Twenty thermocouples were used - two at each of ten axial positions. Six 36-gauge copper-constantan thermocouples were clamped to the inside of the copper shells surrounding the glass tubing. They were spaced directly opposite the odd-numbered tube thermocouple stations. The positions of the stations are given in Table II.

Three 36-gauge copper-constantan thermocouples were taped to the outside of the inlet calming length. As the inlet length was insulated, 210 diameters in length, and operated near room temperature at all times, the wall temperature was taken as the inlet mixed-mean fluid temperature.

The thermocouple voltages were measured with a Rubicon high-precision type B potentiometer using a Leeds and Northrup d-c microvolt amplifier with a zero-center, 50 μv-span meter as a galvanometer. The thermocouple voltages measured were the differences in potential between any thermocouple in question and one of the inlet mixed-mean thermocouples. A cold junction was

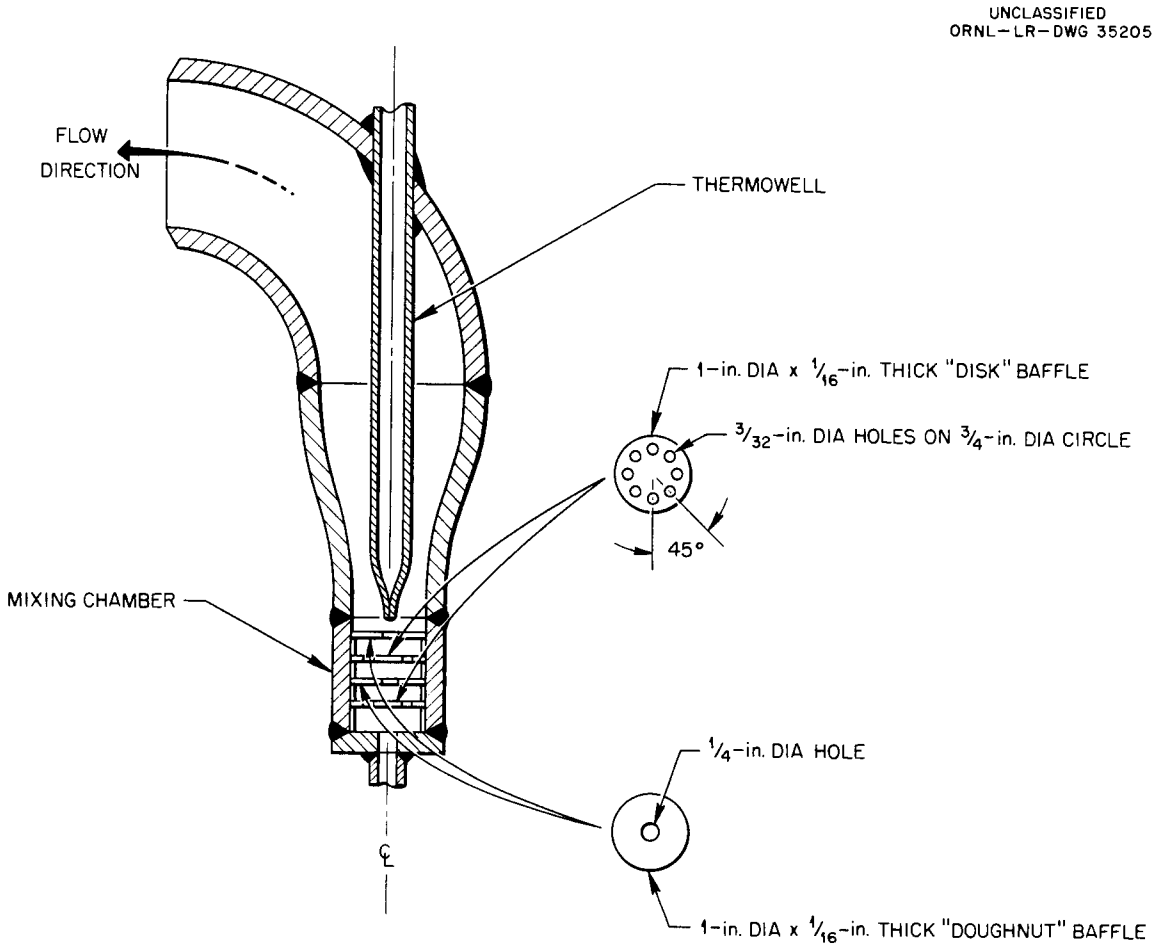

Fig. 6. Cross Section of Exit Mixing Chamber.

TABLE II

POSITIONS OF THERMOCOUPLE STATIONS

Station	Thermocouple		Distance from Centerline of Downstream Electrode (in.)
	On Tube	On Insulation OD	
Exit Mixing Chamber	B-19 (in Thermowell)		
Centerline of Upstream Electrode			16.31
1	B-1, B-13	A-1	14.38
2	A-2, B-2		13.25
3	B-3, B-14	A-3	12.13
4	A-4, B-4		11.00
5	B-5, B-15	A-5	9.88
Centerline of Central Electrode			8.13
6	B-6, B-16	A-6	6.31
7	A-7, B-7		5.19
8	B-8, B-17	A-8	3.69
9	A-9, B-9		2.94
10	B-10, B-18	A-10	1.81
Centerline of Downstream Electrode			0
Inlet Calming Length	B-11		-5.00
	A-11		-10.00
	B-12		-15.00

used to obtain a reference temperature for the inlet mixed-mean thermocouple.

The thermocouple voltages could also be read on a Brown "Electronik" 2-pen recorder, which had a 250°F span.

Electrical Power Circuit

The electrical circuit for resistance heating the mercury is shown in Fig. 7. The power supplied ranged up to 9.57 kw. The power supply consisted of a Superior Electric Powerstat, 0-100 per cent line voltage variation for control, and a low voltage transformer consisting of four powerstat cores connected in a series - parallel arrangement as primaries, and ten turns of two 350 mcm cables in parallel as secondary winding for each core. The resulting over-all transformer ratio was 440:10. The cables were connected in parallel to the test-section bus bars, which split the current equally between two parallel heating circuits. Since the central test-section electrode was at one potential and the two outside electrodes were at the same ground potential, all the heating power was dissipated in the test section between the electrodes. Two window-type current transformers of 1200:5 and 200:5 ratios were placed around the bus bars of each of the two parallel legs of the heating circuit. With these current transformers, two Weston laboratory-type ammeters (0-5 amp scale, 1/2 per cent full-scale accuracy) were used to measure test-section current flow. The test-section voltage drop was measured by a Weston laboratory-type voltmeter (0-3, 7.5, 15, 30, 75, 150, 300, 750 volt ranges, 1/2 per cent of full-scale reading accuracy) connected to taps on the electrodes. The voltage across both legs was measured. Some of the electrical circuit components were visible in Fig. 2 at right rear.

UNCLASSIFIED
ORNL-LR-DWG 35206

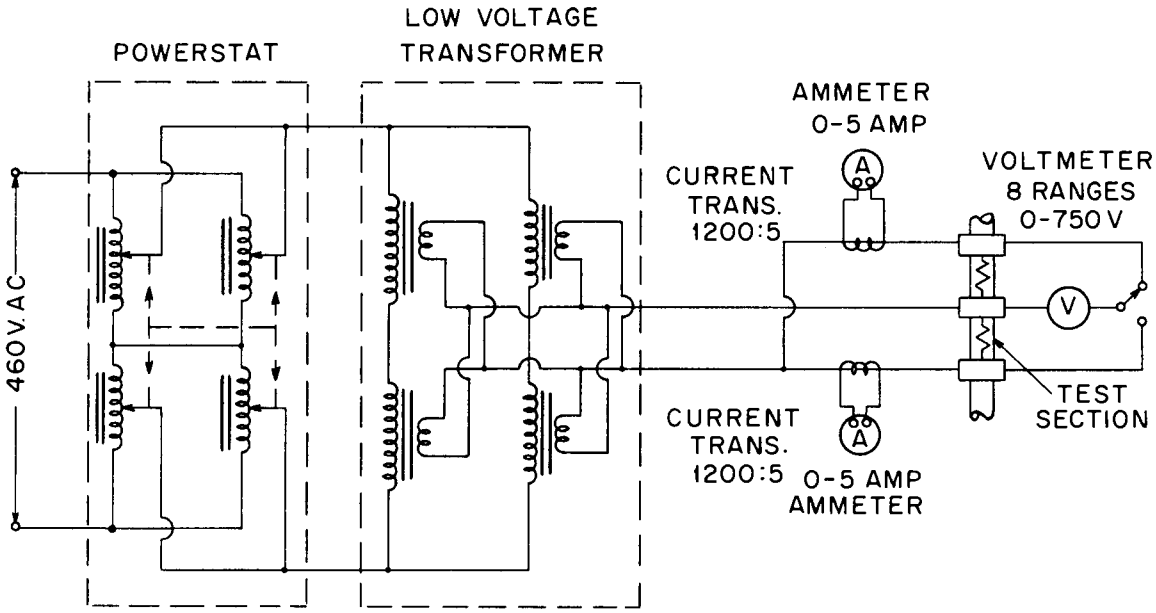

Fig. 7. Electrical Power Circuit

Guard Heaters

Guard heating was employed around the test section to minimize heat losses. Six separately controlled clamshell heaters (hollow cylinders in cross section, wound with coiled Nichrome wire) were spaced along the test section, three on each leg of the test section, as was shown in Fig. 5. A 1/8-in.-thick copper shell between the heaters and the insulation about the test-section tubing served to even out the temperatures generated by the heaters. Unfortunately, the copper was such a good conductor in the axial direction that an axial temperature gradient matching the tube gradient could not be maintained. Consequently, the experiment was run using only the central heater of each of the two legs. Control of the heaters was achieved with Simplytrol controllers using the signal from four copper-constantan thermocouples connected in series; the alternate junctions being on the glass tube wall, and on the inside of the copper shell (see Fig. 4). All junctions were placed at the center of the particular heater being controlled.

The heaters were then controlled to maintain the copper shell temperature at the tube temperatures; this condition gave zero voltage from the thermocouple circuit. When the shell temperatures decreased, the resulting voltage (twice the voltage from a single thermocouple pair) caused power to flow to the guard heater. An increase in shell temperature over the tube temperature turned off the guard heater.

The guard heater power was individually controlled by Variacs such that the shell temperature deviated by ± 3°F from the tube temperature at the control point and the period for a heating and cooling cycle was five minutes or more.

Auxiliary Equipment

Two 1800-watt clamshell-type heaters were placed around the 2-in. pipe carrying mercury between the control valve and the orifice to raise or lower the system temperature. They were controlled individually by Variacs. These were used in conjunction with the mercury cooler to maintain an isothermal condition in the test section at various temperature levels. All of the 2-in. piping in the circuit was insulated to reduce heat losses.

A system of pressure regulators and vent valves connected to the building instrument air supply served to pressurize or vent the surge chamber, sump, and storage tank.

A 3/4-hp oil-sealed vacuum pump was used to evacuate the mercury circuit. It was used to dry the loop after degreasing with perchlorethylene. A vacuum was maintained while the loop was being filled with mercury so that the orifice pressure drop measurement system would be completely filled. A vacuum of 100 μ could be maintained in the dry, empty loop.

Safety circuits included a high-temperature limit which cut off the test-section power if the outlet mercury temperature exceeded 250°F. A low-flow switch attached to the orifice pressure-drop recorder shut off the test-section power if the flow rate dropped below a certain value.

A 2250-lb capacity springless Detecto platform scale having a 1000-lb dial graduated in 1-lb units was used with a small, enclosed, 800-lb capacity tank and an electric timer to calibrate the orifices. The tank and scale are visible in Fig. 2.

A control panel was used to mount the system control equipment and recording instruments. A view of the panel is shown in Fig. 8.

Fig. 8. Control Panel and Instruments.

CHAPTER IV

PROCEDURE

System Preparation

After assembly, the system was thoroughly leak checked while under vacuum using a helium leak detector. The system was subsequently filled with a degreasing agent (perchlorethylene) which was circulated by the pump, drained, and the procedure repeated until the fluid frained appeared clean. The system was then evacuated for several days by the vacuum pump to completely dry the system. The sealant oil in the pump was replaced periodically due to contamination by the perchlorethylene.

The system was then filled under vacuum by transferring mercury from the storage tank. In this manner, the flowmeter lines were completely filled.

Operating Procedure

To start up the equipment, the following steps were taken:

1. Open bypass valve and close all control valves.
2. Turn on air pressure for pump speed control.
3. Start mercury pump.
4. Regulate pump pressure to 70-200 lb/in.^{2} by closing down bypass valve and regulating pump speed.
5. Open and close proper valves in flowmeter tubing to connect desired orifice to high-range differential pressure cell, and set switch to connect cell to strip-chart recorder.

6. Open cutoff valve at sump entrance, and open desired control valve to obtain desired flow rate; connect orifice to low-range cell if required, and set strip-chart recorder switch.
7. Turn on and regulate resistance heating power.
8. Turn on and adjust test-section guard heaters and automatic controls.
9. After system reaches equilibrium, as shown on the thermocouple recorder, record data as follows:
   a. Read orifice pressure drop from strip-chart recorder.
   b. Read test-section voltage and current.
   c. Read thermocouple voltages A-1 through A-15 and then B-1 through B-19 in that order on first the Brown recorder and then the Rubicon potentiometer. All pot voltages were read versus thermocouple B-11; which, in turn, was measured versus an ice-bath junction.

The procedure followed in calibrating the orifices was as follows:

1. After following steps 1 through 4 of the preceding procedure, open exit valve, close cutoff valve, and open desired control valve to regulate flow rate. If necessary, connect orifice to low-range cell and connet cell to strip-chart recorder.
2. After weigh tank begins to fill, start timer and note weight. Read orifice pressure drop, and shut off timer as predetermined weight is reached.
3. When weigh tank is full, transfer mercury back to system by pressuring it through a second hose to the storage tank.

The thermocouple calibration procedure was as follows:

1. Set system flow rate at maximum.
2. Turn on and regulate 1800-watt clamshell heaters and water coolant to obtain desired system temperature.
3. Turn on and regulate guard heaters.
4. After equilibrium has been reached, as indicated on Mueller Bridge, record flow rate, time, and thermocouple voltages (using pot) in following order: junctions B-19, A-1, B-19, A-2, etc., up to B-18. Simultaneously, repeatedly measure resistance of platinum-resistance thermometer. At end of thermocouple measurements, stop resistance thermometer measurements and record time.

Mercury-Sodium Alloy Preparation

Sodium was added to the mercury by first making an alloy of 0.5 w/o Na-Hg in a drybox with a helium atmosphere to prevent oxidation of the sodium. The alloying was done by dropping thumbnail-size pieces of sodium into the mercury. The reaction was quite vigorous, once it started, and considerable heat was evolved. However, the procedure of adding small pieces at sufficiently long intervals kept the alloy temperature down so that the glass container could be handled with asbestos gloves. Subsequent filtration through three layers of cheesecloth removed the small amount of solid sodium oxide which inevitably formed in spite of the helium atmosphere The resulting alloy was then added to the system to make an alloy of 0.02 w/o Na-Hg.

Installation of Test Sections

The glass tubing and electrodes were assembled in the following manner. The electrodes, loosely fastened to the connecting bus bars, were aligned using a plumb bob as a guide. The glass tubing was put in place, and a length of stainless steel tubing machined to an outside diameter of 0.249 in. was inserted through the entire assembly of electrodes and glass tubing. A final alignment of the electrodes was made while checking to see that the gauge tubing moved freely and that the assembly was vertical.

The screw-type glass pipe coupling between the top electrode and the glass tubing was then tightened, and the gauge tube withdrawn from the coupling vicinity. The glass tubing was checked for stresses with a polarized light source. The procedure was repeated for each coupling in turn; the gauge tube being used to align the parts. A final, visual check was made by looking up through the bore. The glass tubing was then loaded in compression by tension rods connecting the bus bars coupled to the electrodes. Then the bus bars were clamped to the supporting framework. Finally, the entrance calming length was coupled on. No alignment was possible here, but it was felt that any misalignment would be small and that any resulting effects would be evened out in the 70-dia length of test section. The glass sections were then given a final check for stresses. The glass was cleaned with carbon tetrachloride prior to installation.

CHAPTER V

THE MEASUREMENTS

Results

Several test runs were made to determine wall to mixed-mean fluid temperature differences for the variety of flow rates and power densities shown in Table III. The range of Reynolds moduli was from 29,000 to 164,500. Because of flow rate control difficulties, it was impossible to obtain meaningful data at lower flow rates. The results are plotted in dimensionless form in Fig. 9. A typical set of test-section temperatures is shown in Fig. 10 as a function of test-section length. The mixed-mean fluid temperature curve was derived using the measured resistance of each test-section leg and the average resistivity of the mercury in each leg. Thus, the heated length of each leg was calculated. The unheated portions of the test section were assumed equal in length. All the heat was assumed to be generated in the calculated length. The cross-sectional area through which the current flowed into the mercury in the electrodes was about ten times the mercury cross-sectional area. This would make the current density in the electrode roughly one-tenth of the test-section current density and thus make the power density in the mercury in the electrode 0.01 times the test-section power density. Also, since the copper bus bar is a much better conductor than mercury, the current density at the electrode edges will be high and close to zero at the center of the electrode. It is seen that the assumption made is a very good approximation.

TABLE III

EXPERIMENTAL RESULTS

Run No.	Volumetric Heat Generation Rate, q''', Btu/hr·ft^3	N_{Re}	N_{Pr}	Electrical Power Input, q_{in}, Btu/hr	Heat Removed from Test Section q_{out}, Btu/hr	$\frac{q_{in}}{q_{out}}$	Axial Temp. Rise, °F	Radial Temp. Dif., $t_w - t_m$, °F
1	3.48×10^7	73,300	0.0200	13,880	13,040	0.939	104.47	3.46
2	1.65×10^7	29,000	0.0200	6,700	6,060	0.905	127.05	3.90
3	2.55×10^7	45,200	0.0200	9,940	10,280	0.969	125.51	4.90
4	7.53×10^7	147,000	0.0192	29,500	27,400	0.929	113.35	4.08
6	5.84×10^7	102,900	0.0192	22,670	20,530	0.907	125.41	3.25
11	8.30×10^7	164,500	0.0191	32,700	29,900	0.915	113.30	5.87
12	5.10×10^7	95,700	0.0200	20,600	18,100	0.878	119.03	4.57
13	2.68×10^7	88,500	0.0225	10,870	9,710	0.894	63.71	2.23
14	3.20×10^7	58,400	0.0205	13,060	11,860	0.908	122.42	3.33
15	2.25×10^7	40,000	0.0204	9,060	8,510	0.939	124.11	2.83
16	1.44×10^7	39,200	0.0224	5,660	5,200	0.919	75.49	1.81
17	6.51×10^7	124,000	0.0207	26,450	24,100	0.911	116.46	5.78

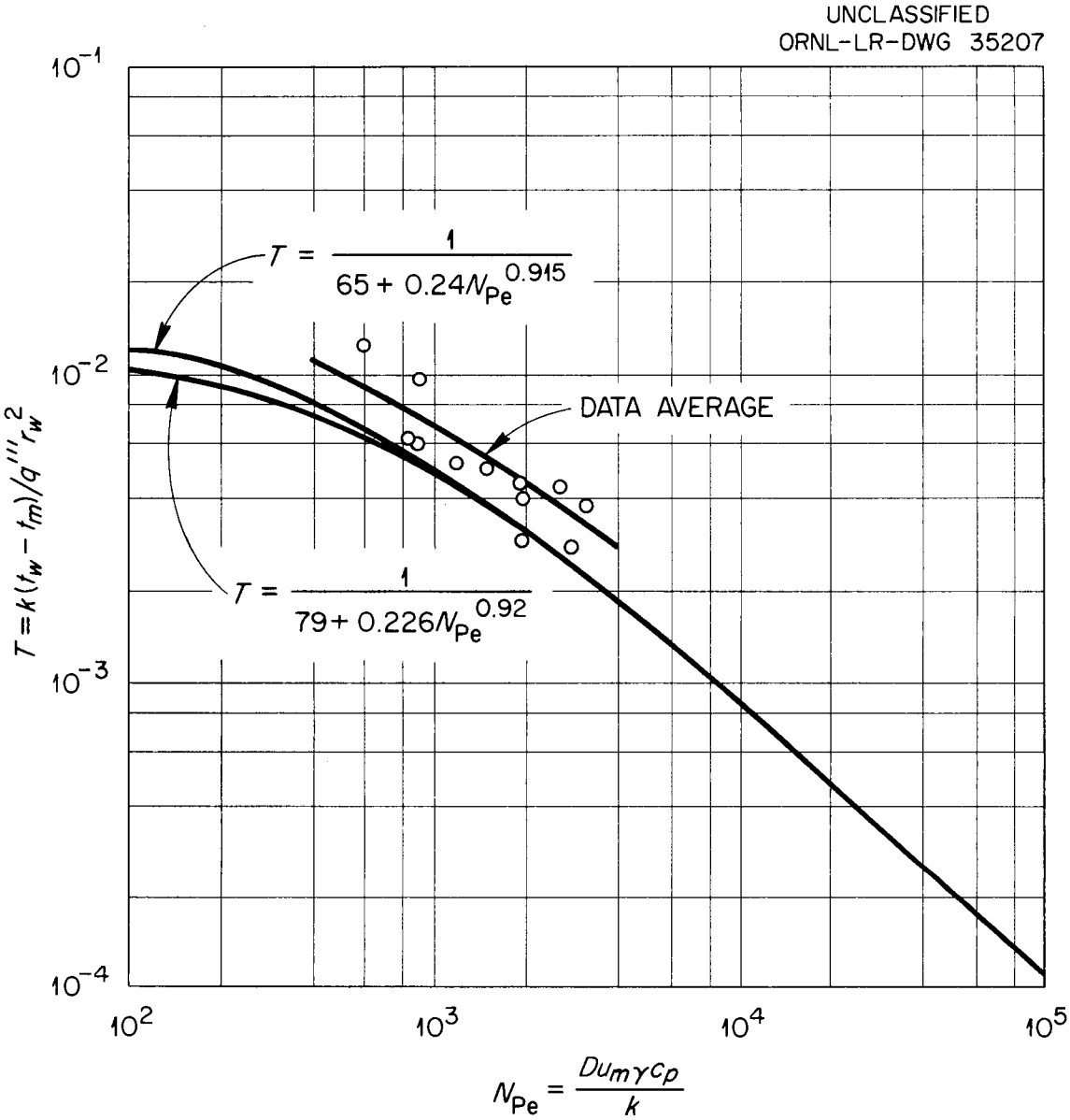

Fig. 9. Theoretical and Experimental Differences Between Wall and Mixed-Mean Fluid Temperatures With Insulated Wall.

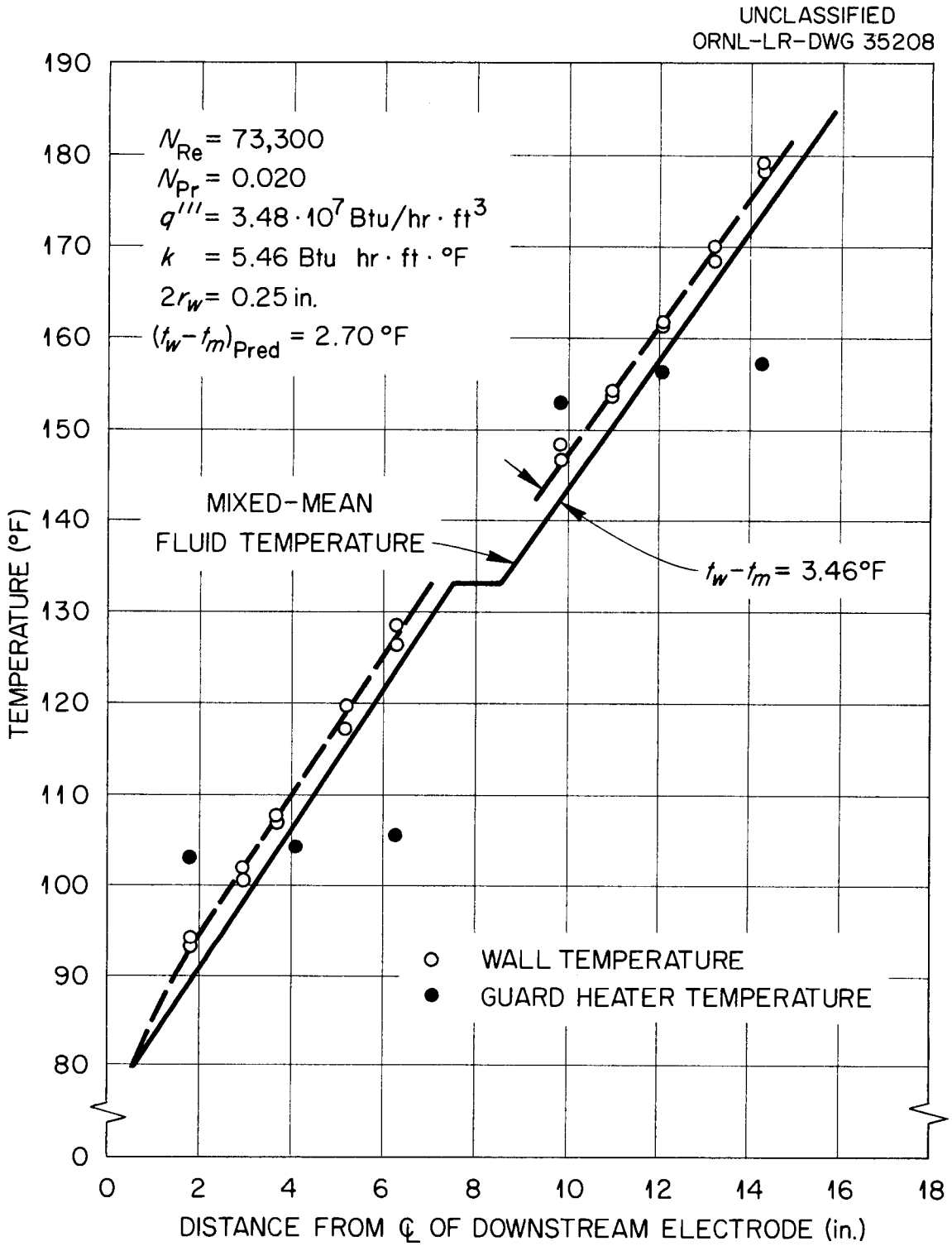

Fig. 10 Typical Experimental Temperatures in Test Section.

Errors in the Measurements

Heat balances were consistently low; the heat removed from the test section being between 89.8 per cent and 96.8 per cent of the electrical power input.

The accountable errors in the heat balance are listed below:

A. Power

Two voltage readings at ± 2 per cent

Two current readings at ± 2 per cent

Maximum error = 1.02 x 1.02 + 1.02 x 1.02 = 1.08

0.98 x 0.98 + 0.98 x 0.98 = 0.92

Maximum error = ± 8 per cent

B. Heat Removed

Δp maximum error ± 5 per cent

Error in calibrated coefficient ± 6 per cent

Maximum error in flow rate $\propto C\sqrt{\Delta p}$ ± 8.5 per cent

Δt maximum error = $\pm \frac{0.5°F}{100°F}$ = ± 0.5 per cent

Maximum error in heat removed ± 8.6 per cent

The variations of measured test-section resistance were about ± 4 per cent at the maximum. This is accounted for by the voltage and current measurement errors, which could have caused a ± 4 per cent error.

Since the heat losses were much smaller than the apparent differences in the heat balance, as determined by some isothermal runs, the discrepancy was ascribed to the flow rate measurement. The differential pressure cell-recorder system was subject to shifts in the zero reading, which could come either from accidentally operating the cell at a greater-than-maximum Δp or from air bubbles in the lines leading to the orifices.

The power input was subsequently used to determine the flow rate in conjunction with the measured Δt and the average heat capacity of the mercury. In any case, the final result shown in Fig. 9 will not change markedly since a change in flow rate changes the power density, and thus moves a data point along a straight line almost parallel to the predictions and the correlation. Thus, the scatter of the data is due primarily to the small radial temperature differences encountered ($\sim$ 2 to 6°F).

Despite the calibration in position of the thermocouples, the temperatures were probably accurate to ± 0.4°F. This would mean that the temperature differences were accurate to $\pm \frac{0.8}{2}$, or ± 40 per cent at the very worst. Inspection of Fig. 9 or Table III shows a ± 35 per cent maximum variation from the mean of the data. Thus, the errors appear to be accounted for.

Auxiliary Measurements

The thin-plate orifices were calibrated by pumping mercury through them, and into a weigh tank. The resulting coefficients are shown in Table IV. The maximum deviation from the coefficients listed in Table IV was ± 7.5 per cent. Most of the calibration data was within ± 3 per cent of the coefficients.

The thermocouples were calibrated in position by placing a Bureau of Standards calibrated Leeds and Northrup No. 8163 platinum-resistance thermometer in the exit mixing chamber thermowell with the thermocouple, and operating the test section isothermally at 58, 118, 148, and 222°F.

After the test section reached a reasonable state of equilibrium, the resistance thermometer was read repeatedly using a Leeds and Northrup

TABLE IV

ORIFICE COEFFICIENTS

Orifice	Orifice Diameter (in.)	Pipe Diameter (in.)	Coefficient
1	0.081	1.049	0.562
2	0.255	1.049	0.558
3	0.741	1.049	0.666

type G-2 Mueller Bridge. During this time, the exit mixing chamber thermocouple was read on the potentiometer alternately with each of the other test-section thermocouples. In this manner, a comparison could be made between the test-section thermocouples and the resistance thermometer. Since the fluid velocity in the test section was about 1.5 ft/sec and the fluid mixed-mean temperature did not change faster than 0.2°C/min or more than 0.6°C over a test-run period of 30 min, the comparison was good.

The guard heaters were used to insure minimum heat loss. The effect of guard heater temperature on the test-section thermocouples was tested by running the system with high flow rates and large Δt's between heater and test-section wall. By calculating a heat-transfer coefficient for the mercury and using the temperature difference between the outside of the tube and the bulk mercury, the mercury-tube interface temperature was computed, knowing the glass thermal conductivity. Thus, a ratio of guard heater-outside tube wall Δt to outside tube wall-inside tube wall Δt was found. This correction ratio was applied to the calibration data, and also to the power-run data.

The calibration data were also applied to the test-section thermocouple measurements. However, despite these corrections, the thermocouple measurements were probably accurate only to within ± 0.4°F because of spurious signals sometimes introduced by the guard heater control system. The corrected thermocouple calibration data are shown in Fig. 11.

Since the six central thermocouples of the upstream half of the test section were relatively free of end effects due to the massive electrodes, the average value of the wall-fluid temperature differences at these points was used in Table III and Fig. 9.

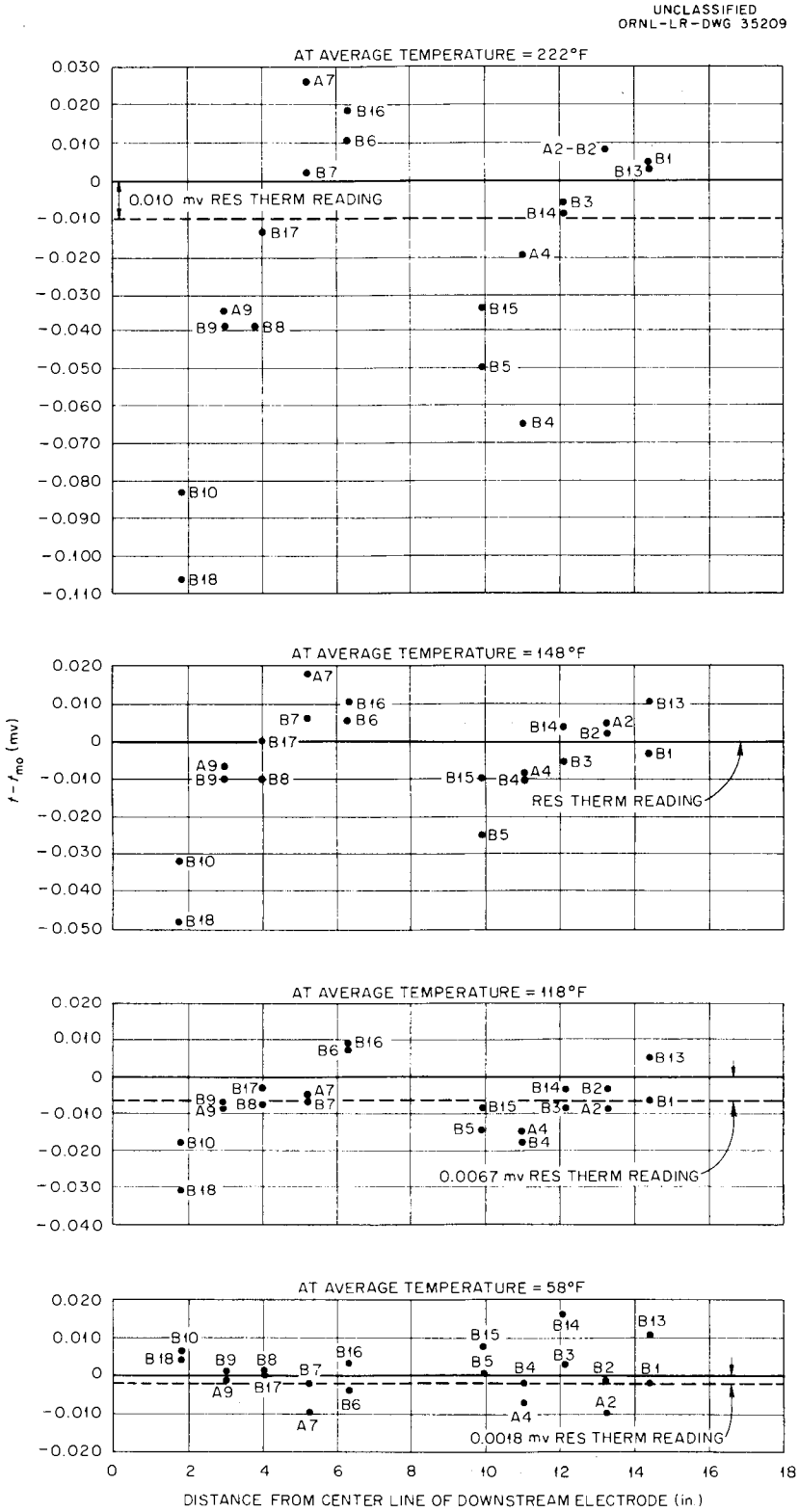

Fig. 11. Corrected Thermocouple Calibrations.

The electrical resistance of the test section was not appreciably changed by the presence of the copper shields around the test section, as was shown by resistance measurements with and without the shields.

CHAPTER VI

DISCUSSION

Discussion of Experimental Results

It is seen from Fig. 9 that the measured temperature difference parameters are, on the average, 49 per cent higher than the predictions of Poppendiek based on the heat-momentum transfer analogy. An empirical correlation of the data was given by:

$$T = \frac{1}{53.0 + 0.152\, N_{Pe}^{0.92}} \tag{35}$$

The maximum deviation of the data from the correlation was approximately ± 35 per cent. The standard deviation was ± 24 per cent. Much of this deviation was due to the small radial temperature differences encountered.

The properties of mercury were taken from reference 14.

That the effect on heat transfer of the magnetic and electric fields generated by the large heating currents (about 400 to 950 amp per leg) was essentially negligible can be seen by comparing runs 12 to 13 and 15 to 16 of Table III. The magnetic field strength was changed by a factor of two between runs 12 and 13, and between runs 15 and 16, and no appreciable differences were found. This result was confirmed by a rough analysis using the results of Murgatroyd[15] for magnetohydrodynamic channel flow. The maximum change in the friction coefficient for the field strengths encountered here was estimated to 2 per cent. The heat transfer should be affected by roughly the same amount.

Since no heat was transferred through the test-section wall, interfacial resistances (gas films or scales) cannot affect the results. Thus, it may be concluded that, on the average, the radial conductances are smaller than those calculated from the heat-momentum transfer analogy. This is essentially the same result as ordinary heat-transfer tests with liquid metals have shown.[16] Thus, it appears that the ratio α is not unity but somewhat smaller. Though this avenue of inquiry was not explored here, others[17,18] have proposed heat-momentum transfer analogies where α is a function of Prandtl number. From the experiments of Isakoff and Drew,[19] and Brown and Short,[20] it appears that α is also a function of radial position and Reynolds number, though there was wide disagreement as to the values of α.

It would be interesting to apply these newer theories to volume-heat-source heat transfer in liquid metals to see if the predictions are improved over the theory expounded here. Since the radial heat flow is much different in volume-heat-source heat transfer and ordinary heat transfer, perhaps additional discrepancies would appear because of the apparent dependence of α upon radial position.

In this connection, the equipment was originally designed for much larger diameter test sections (1.5-in. ID) so that the mercury stream could be proved for temperature and velocity distributions to obtain diffusivities of heat and momentum. It is hoped that this part of the investigation will be pursued by Oak Ridge National Laboratory in the future.

CHAPTER VII

CONCLUSIONS

The experimental investigation conducted has revealed the same discrepancy between theory (based on the Martinelli heat-momentum transfer analogy) and experiment as observed in many studies of ordinary wall heat transfer with liquid metals.[16] Since no heat was transferred across the wall, interfacial resistances (gaseous or solid films) could not affect the results. Therefore, it was concluded that the molecular and/or eddy diffusivities of heat were, on the average, smaller than predicted by the above analogy.

The experimental data was empirically correlated by the equation:

$$T = \frac{1}{53.0 + 0.152\, N_{Pe}^{0.92}} \tag{36}$$

It was shown that Poppendiek's analytical results for heat transfer with internal heat generation reduced to the integral equation of Lyon for the case of no internal heat generation. It was then possible to express the effect of internal heat generation on the heat-transfer coefficient by the equation:

$$\frac{1}{N_{Nu}^{*}} = \frac{1}{N_{Nu}} + \frac{q_f}{q_w} T \tag{37}$$

Thus, the presence of internal heat generation increases the effective Nusselt modulus for cooling and decreases it for heating.

Further, since with internal heat generation only a small portion of the total heat passes through the high thermal resistance region near

the wall, it was found that smaller wall-fluid temperature differences resulted than with the flow of the same quantity of heat through the wall. This then explains Stromquist's results for mercury heat transfer wherein it was found that the Nusselt modulus decreased only 0.5 per cent although 6 per cent of the total test-section heat generation occurred in the mercury.

Since α has been shown to be less than unity, it is recommended that the theories of Jenkins[17] and Lykoudis and Touloukian[18] be applied to volume-heat-source heat transfer. The differences in radial heat flow in this system and in ordinary heat-transfer systems may allow clearer delineation of the apparent dependence of α on radial position.

It was also recommended that further studies of the internal temperature and velocity distributions in this type of system be made.

LIST OF REFERENCES

LIST OF REFERENCES

1. Goldstein, S., Ed., "Modern Developments in Fluid Dynamics," Vol. II, Oxford University Press, Amen House, London, E. C. 4, p 651 (1938)

2. Prandtl, L., Physik. Zeitschr., 29, pp 487-489 (1928)

3. Poppendiek, H. F., "Forced-Convection Heat Transfer in Pipes with Volume Heat Sources within the Fluids," Chem. Eng. Prog. Symposium Series, Vol. 50, No. 11, pp 93-104 (1954)

4. Hamilton, D. C., et al., "Free-Convection in Fluids Having a Volume Heat Source," ORNL-1769 (1954)

5. Hamilton, D. C., and Lynch, F. E., "Free-Convection Theory and Experiment in Fluids Having a Volume Heat Source," ORNL-1888 (1955)

6. Poppendiek, H. F., "A Laminar Forced-Convection Solution for Pipes Ducting Liquids Having Volume Heat Sources and Large Radial Differences in Viscosity," ORNL-CF 54-11-37 (1954)

7. Poppendiek, H. F., and Palmer, L. D., "Forced-Convection Heat Transfer Between Parallel Plates and in Annuli with Volume Heat Sources within the Fluids," ORNL-1701 (1954)

8. Poppendiek, H. F., and Palmer, L. D., "Application of Temperature Solutions for Forced-Convection Systems with Volume Heat Sources to General Convection Problems," ORNL-1933 (1955)

9. Poppendiek, H. F., "Heat Transfer within the Cores of Circulating-Fuel Reactors," Reactor Heat Transfer Conference of 1956, TID-7529 (Part I), Book 1, pp 262-272 (Ussued November 1957)

10. Hallman, T. M., "Combined Forced- and Free-Laminar Heat Transfer in Vertical Tubes with Uniform Internal Heat Generation," Trans. ASME, pp 1831-1841 (Nov. 1956)

11. Martinelli, R. C., "Heat Transfer to Molten Metals," Trans. ASME, pp 947-959 (Nov. 1947)

12. Lyon, R. N., "Liquid Metal Heat-Transfer Coefficients," Chem. Eng. Prog., Vol. 47, No. 2., pp 75-79 (Feb. 1951)

13. Stromquist and Boarts, "Effects of Wetting on Liquid Metal Heat Transfer," ORO-93, TISE, USAEC, Oak Ridge (1953)

14. Lyon, R. N., Ed., "Liquid Metals Handbook," 2nd Ed., NAVEXOS, p 733 (Rev.) (June 1952)

15. Murgatroyd, W., "Experiments on Magneto-Hydrodynamic Channel Flow," Philosophical Mag., pp 1348-1354 (1953)

16. Lubarsky, B., and Kaufman, S. J., "Review of Experimental Investigations of Liquid Metal Heat Transfer," NACA-1270 (1956)

17. Jenkins, R., "Variation of the Eddy Conductivity with Prandtl Modulus and its use in Prediction of Turbulent Heat-Transfer Coefficients," Heat Trans. & Fl. Mech. Inst., Stanford Univ., Stanford, Calif., pp 147-158 (1951)

18. Lykoudis, P. S., and Touloukian, Y. S., "Heat Transfer in Liquid Metals," Trans. ASME, pp 653-666, (April 1958)

19. Isakoff, S. E., and Drew, T. B., "Heat and Momentum Transfer in Turbulent Flow of Mercury," General Discussion on Heat Transfer, Inst. Mech. Eng. and ASME, pp 405-409 (1951)

20. Amstead, B. H., Brown, H. E., and Short, B. E., "Temperature and Velocity Distribution and Transfer of Heat in a Liquid Metal," Trans. ASME, p 279 (Feb. 1957)

APPENDIX

APPENDIX

A. NUMERICAL CALCULATIONS OF PREDICTED VALUES FOR T FOR LIQUID METALS

The equations used in these calculations were taken from the calculations of Poppendiek.[3]

The radial heat flow relationships are:

For $0 \leq n \leq 158/N_{Re}^{0.9}$

$$\frac{\frac{dq}{dA}}{q''' r_w} = \frac{1}{1 - n} \int_0^n 0.0115\, N_{Re}^{0.8}\, n\,(1 - n)\, dn + \frac{n\,(n - 2)}{2\,(1 - n)}$$

$$\frac{\frac{dq}{dA}}{q''' r_w} = \frac{0.0115\, N_{Re}^{0.8}}{1 - n} \left[\frac{n^2}{2} - \frac{n^3}{3} \right] + \frac{n\,(n - 2)}{2\,(1 - n)} \tag{38}$$

For $158/N_{Re}^{0.9} \leq n \leq 1$

$$\frac{\frac{dq}{dA}}{q''' r_w} = \left[\frac{1 - 158/N_{Re}^{0.9}}{1 - n} \right] \frac{\left(\frac{dq}{dA}\right)_{n = 158/N_{Re}^{0.9}}}{q''' r_w}$$

$$+ \frac{f}{1 - n} \left[\frac{7}{8} n^{8/7} - \frac{7}{15} n^{15/7} \right]_{158/N_{Re}^{0.9}}^{n} \tag{39}$$

$$+ \frac{\left[-2n + n^2 + 2\,\frac{158}{N_{Re}^{0.9}} - \left(\frac{158}{N_{Re}^{0.9}}\right)^2 \right]}{2\,(1 - n)}$$

where

$$f = \frac{1 - 0.023\, N_{Re}^{0.8} \left[\frac{1}{2}\left(158/N_{Re}^{0.9}\right)^2 - \frac{1}{3}\left(158/N_{Re}^{0.9}\right)^3 \right]}{2\left[\frac{49}{120} - \frac{7}{8}\left(158/N_{Re}^{0.9}\right)^{8/7} + \frac{7}{15}\left(158/N_{Re}^{0.9}\right)^{15/7} \right]} \tag{40}$$

The calculation of the temperature differences were divided into four regions: the laminar sublayer, the buffer layer, and the outer and inner turbulent layers. The eddy diffusivities for these regions are as follows:

Laminar Sublayer,

$$0 \leq n \leq 66/N_{Re}^{0.9} = n_1 \quad , \quad \frac{\epsilon_m}{\nu} = 0$$

Buffer Layer,

$$n_1 \leq n \leq 396/N_{Re}^{0.9} = n_2 \quad , \quad \frac{\epsilon_m}{\nu} = 0.0152\, N_{Re}^{0.9}\, (n - 1)$$

Outer Turbulent Core,

$$n_2 \leq n \leq 0.5 \quad , \quad \frac{\epsilon_m}{\nu} = 0.0304\, N_{Re}^{0.9}\, (1 - n)\, n$$

Inner Turbulent core,

$$0.5 \leq n \leq 1.0 \quad , \quad \frac{\epsilon_m}{\nu} = 0.0076\, N_{Re}^{0.9}$$

The equations are (letting $(dq/dA)/q'''\, r_w = \Phi$):

Laminar Sublayer,

$$\frac{k\,(t - t_w)}{q'''\, r_w^2} = \int_0^n \Phi\, dn \quad , \quad 0 \leq n \leq n_1 \tag{41}$$

Buffer Layer,

$$\frac{k\,(t - t_{n_1})}{q'''\, r_w^2} = \int_{n_1}^{n} \frac{\Phi\, dn}{1 - N_{Pr} + 0.0152\, N_{Pr}\, N_{Re}^{0.9}\, n} \quad , \quad n_1 \leq n \leq n_2 \tag{42}$$

Outer Turbulent Layer,

$$\frac{k\,(t - t_{n_2})}{q'''\,r_w^{\,2}} = \int_{n_2}^{n} \frac{\Phi\,dn}{1 + 0.0304\,N_{Pr}\,N_{Re}^{0.9}\,(n - n^2)} \quad , \; n_2 \leq n \leq 0.5 \qquad (43)$$

Inner Turbulent Layer,

$$\frac{k\,(t - t_{0.5})}{q'''\,r_w^{\,2}} = \int_{0.5}^{n} \frac{\Phi\,dn}{1 + 0.0076\,N_{Pr}\,N_{Re}^{0.9}} \quad , \qquad 0.5 \leq n \leq 1.0 \qquad (44)$$

All integrals were numerically evaluated by the trapezoidal rule.

The calculation of $k\,(t_w - t_{\mathbb{C}})/q'''\,r_w^{\,2}$ is then made by summing the results of the four layers, and $(t_w - t_m)$ is then calculated from the equation:

For $N_{Re} = 5000$

$$\frac{k\,(t_w - t_m)}{q'''\,r_w^{\,2}} = 2\int_{\left(1 - \frac{158}{N_{Re}^{0.9}}\right)}^{1} 0.0115\,N_{Re}^{0.8}\,(1 - S)\,S\left[\frac{k\,(t_w - t)}{q'''\,r_w^{\,2}}\right] dS$$

$$+ \int_{0}^{\left(1 - \frac{158}{N_{Re}^{0.9}}\right)} fS\,(1 - S)^{1/7}\left[\frac{k\,(t_w - t)}{q'''\,r_w^{\,2}}\right] dS \qquad (45)$$

For N_{Re} = 10,000, 100,000, and 1,000,000

$$\frac{k\,(t_w - t_m)}{q'''\,r_w^{\,2}} = \frac{k\,(t_w - t_{\mathbb{C}})}{q'''\,r_w^{\,2}} - \frac{120}{49}\int_{0}^{1} \frac{k\,(t - t_{\mathbb{C}})}{q'''\,r_w^{\,2}}\,(1 - S)^{1/7}\,S\,dS \qquad (46)$$

Equations (45) and (46) were integrated graphically with a planimeter. Table V shows the values of $(dq/dA)/q_m'''\,r_w$ as obtained from equations (38) and (39). Tables VI through IX show the numberical computations using the

TABLE V

VALUES* OF THE FUNCTION, $\frac{\frac{dq}{dA}}{q'''\ r_w} = \phi$

N_{Re} = 5,000		N_{Re} = 10,000		N_{Re} = 100,000		N_{Re} = 1,000,000	
n	ϕ	n	ϕ	n	ϕ	n	ϕ
0.005	-0.004987	0.005	-0.004772	0.0005	-0.000486	0.00005	-0.00004910
0.010	-0.009424	0.010	-0.009238	0.0010	-0.000943	0.00010	-0.00009638
0.015	-0.01391	0.013	-0.01156	0.0015	-0.001471	0.00020	-0.0001855
0.03095	-0.02637	0.01658	-0.01420	0.002087	-0.001839	0.0002627	-0.000238
0.05	-0.03800	0.025	-0.01958	0.003	-0.002487	0.0004	-0.000342
0.06	-0.04267	0.032	-0.02309	0.004	-0.003087	0.0005	-0.000412
0.08	-0.04847	0.05	-0.02825	0.004996	-0.003571	0.0006290	-0.000486
0.11	-0.05243	0.06	-0.03026	0.007	-0.004400	0.0008	-0.000582
0.15	-0.05630	0.08	-0.03378	0.01	-0.005553	0.0010	-0.000693
0.1856	-0.05868	0.09947	-0.03667	0.01253	-0.00646	0.001577	-0.000997
0.20	-0.05941	0.15	-0.04239	0.05	-0.01780	0.004	-0.002149
0.25	-0.06106	0.20	-0.04613	0.10	-0.02547	0.01	-0.004566
0.30	-0.06150	0.25	-0.04846	0.15	-0.03157	0.05	-0.01563
0.40	-0.05959	0.35	-0.04983	0.25	-0.03865	0.15	-0.03067
0.45	-0.05744	0.40	-0.04920	0.30	-0.04035	0.20	-0.03494
0.50	-0.05464	0.45	-0.04783	0.35	-0.04115	0.25	-0.03783
0.55	-0.05122	0.50	-0.04584	0.40	-0.04111	0.30	-0.03958
0.60	-0.04726	0.55	-0.04324	0.45	-0.04036	0.35	-0.04043
0.65	-0.04281	0.60	-0.04011	0.50	-0.03899	0.40	-0.04044
0.70	-0.03789	0.65	-0.03651	0.55	-0.03703	0.45	-0.03973
0.75	-0.03250	0.70	-0.03246	0.60	-0.03455	0.50	-0.03842
0.80	-0.02672	0.75	-0.02795	0.65	-0.03162	0.55	-0.03651
0.85	-0.02051	0.80	-0.02306	0.70	-0.02824	0.60	-0.03409
0.90	-0.01399	0.85	-0.01775	0.75	-0.02441	0.70	-0.02789
0.95	-0.00727	0.90	-0.01214	0.80	-0.02021	0.75	-0.02411
1.00	0	0.95	-0.00634	0.85	-0.01561	0.80	-0.01997
		1.00	0	0.90	-0.01070	0.85	-0.01543
				0.95	-0.00561	0.90	-0.01058
				1.00	0	0.95	-0.00555
						1.00	0

*Obtained from H. F. Poppendiek.[3]

TABLE VI

CALCULATION OF TEMPERATURE DIFFERENCES FOR $N_{Re} = 5000$

For all N_{Pr} / n	Laminar Sublayer $\int_0^n \Phi \, dn$
0.005	-0.0000121
0.015	-0.0001071
0.025	-0.0002878
n_1= 0.03095	-0.0004331

N_{Pr} / n	Buffer Layer $\frac{\Phi}{1 - N_{Pr} + 0.0152\, N_{Pr}\, N_{Re}^{0.9}\, n}$					$\int_{n_1}^{n} \frac{\Phi \, dn}{1 - N_{Pr} + 0.0152\, N_{Pr}\, N_{Re}^{0.9}\, n}$				
	0.002	0.005	0.020	0.050	0.100	0.002	0.005	0.020	0.050	0.100
n_1 = 0.03095	-0.0264	-0.0264	-0.0264	-0.0264	-0.0264					
0.05	-0.0380	-0.0379	-0.0375	-0.0369	-0.0358	-0.000617	-0.000613	-0.000610	-0.000602	-0.000592
0.06	-0.0426	-0.0425	-0.0419	-0.0407	-0.0390	-0.001019	-0.001014	-0.001007	-0.000990	-0.000966
0.08	-0.0483	-0.0481	-0.0470	-0.0449	-0.0418	-0.001936	-0.001925	-0.001900	-0.001852	-0.001779
0.11	-0.0522	-0.0518	-0.0499	-0.0465	-0.0417	-0.003444	-0.003423	-0.003353	-0.003222	-0.003032
0.15	-0.0559	-0.0552	-0.0523	-0.0472	-0.0416	-0.005604	-0.005563	-0.005395	-0.005095	-0.004679
n_2 = 0.1856	-0.0581	-0.0572	-0.0533	-0.0469	-0.0391	-0.007633	-0.007564	-0.007275	-0.006770	-0.006098

TABLE VI (Continued)

CALCULATION OF TEMPERATURE DIFFERENCES FOR $N_{Re} = 5000$

N_{Pr} / n	Outer Turbulent Layer: $\frac{\phi}{1 + 0.0304\, N_{Pr}\, N_{Re}^{0.9}\,(n - n^2)}$					$\int_{n_2}^{n} \frac{\phi\, dn}{1 + 0.0304\, N_{Pr}\, N_{Re}^{0.9}\,(n - n^2)}$				
	0.002	0.005	0.020	0.050	0.100	0.002	0.005	0.020	0.050	0.100
$n_2 = 0.1856$	-0.0576	-0.0559	-0.0491	-0.0394	-0.0296					
0.2	-0.0582	-0.0565	-0.0492	-0.0391	-0.0292					
0.25	-0.0596	-0.0576	-0.0491	-0.0380	-0.0276					
0.3	-0.0599	-0.0576	-0.0483	-0.0366	-0.0260	-0.00676	-0.00653	-0.00561	-0.00435	-0.00318
0.35	-0.0592	-0.0568	-0.0471	-0.0351	-0.0246					
0.4	-0.0578	-0.0553	-0.0454	-0.0335	-0.0233	-0.01264	-0.01218	-0.01030	-0.00785	-0.00565
0.45	-0.0557	-0.0532	-0.0435	-0.0319	-0.0221					
0.5	-0.0529	-0.0505	-0.0413	-0.0302	-0.0208	-0.01818	-0.01747	-0.01463	-0.01103	-0.00786

N_{Pr} / n	Inner Turbulent Layer: $\frac{\phi}{1 + 0.0076\, N_{Pr}\, N_{Re}^{0.9}}$					$\int_{n_2}^{n} \frac{\phi\, dn}{1 + 0.0304\, N_{Pr} N_{Re}^{0.9}(n - n^2)} + \int_{0.5}^{n} \frac{\phi\, dn}{1 + 0.0076\, N_{Pr} N_{Re}^{0.9}}$				
	0.002	0.005	0.020	0.050	0.100	0.002	0.005	0.020	0.050	0.100
0.5	-0.0529	-0.0505	-0.0413	-0.0302	-0.0208	-0.01818	-0.01747	-0.01463	-0.01103	-0.00786
0.55	-0.0496	-0.0474	-0.0387	-0.0283	-0.0195					
0.6	-0.0458	-0.0437	-0.0357	-0.0261	-0.0180	-0.02311	-0.02228	-0.01848	-0.01385	-0.00980
0.65	-0.0415	-0.0396	-0.0323	-0.0236	-0.0163					
0.7	-0.0367	-0.0351	-0.0286	-0.0209	-0.0145					
0.75	-0.0315	-0.0301	-0.0245	-0.0180	-0.0124					
0.8	-0.0259	-0.0247	-0.0202	-0.0148	-0.0102	-0.03028	-0.02912	-0.02407	-0.01793	-0.01263
0.85	-0.0199	-0.0190	-0.0155	-0.0113	-0.0078					
0.9	-0.0136	-0.0129	-0.0106	-0.0077	-0.0053					
0.95	-0.0074	-0.0067	-0.0055	-0.0040	-0.0028					
1.00	0	0	0	0	0	-0.03287	-0.03160	-0.02608	-0.01941	-0.01364

TABLE VII

CALCULATION OF TEMPERATURE DIFFERENCES FOR N_{Re} = 10,000

For all N_{Pr} / n	Laminar Sublayer									
						$\int_0^n \phi \, dn$				
0.005						-1.106×10^{-4}				
0.010						-4.585×10^{-4}				
0.013						-7.689×10^{-4}				
n_1 = 0.01658						-13.048×10^{-4}				
	Buffer Layer									
N_{Pr}	$\frac{\phi}{1 - N_{Pr} + 0.0152\, N_{Pr}\, N_{Re}^{0.9}\, n}$					$\int_{n_1}^n \frac{\phi \, dn}{1 - N_{Pr} + 0.0152\, N_{Pr}\, N_{Re}^{0.9}\, n}$				
n	0.002	0.005	0.020	0.050	0.100	0.002	0.005	0.020	0.050	0.100
n_1 = 0.01658	-0.0142	-0.0142	-0.0142	-0.0142	-0.0142	-0.000142	-0.000142	-0.000141	-0.000140	-0.000138
0.025	-0.0196	-0.0195	-0.0194	-0.0191	-0.0186	-0.000246	-0.000246	-0.000245	-0.000241	-0.000236
0.032	-0.0231	-0.0230	-0.0227	-0.0221	-0.0211	-0.000485	-0.000485	-0.000479	-0.000468	-0.000453
0.05	-0.0281	-0.0280	-0.0272	-0.0257	-0.0235	-0.000754	-0.000752	-0.000740	-0.000717	-0.000684
0.06	-0.0301	-0.0299	-0.0287	-0.0267	-0.0240	-0.001045	-0.001041	-0.001020	-0.000979	-0.000921
0.08	-0.0335	-0.0331	-0.0314	-0.0283	-0.0244	-0.001681	-0.001671	-0.001621	-0.001529	-0.001405
n_2 = 0.09947	-0.0363	-0.0358	-0.0333	-0.0293	-0.0244	-0.002361	-0.002342	-0.002251	-0.002091	-0.001880

TABLE VII (Continued)

CALCULATION OF TEMPERATURE DIFFERENCES FOR N_{Re} = 10,000

N_{Pr} / n	Outer Turbulent Layer: $\frac{\phi}{1 + 0.0304\, N_{Re}\, N_{Pr}^{0.9}\,(n - n^2)}$					Outer Turbulent Layer: $\int_{n_2}^{n} \frac{\phi\, dn}{1 + 0.0304\, N_{Re}\, N_{Pr}^{0.9}\,(n - n^2)}$				
	0.002	0.005	0.020	0.050	0.100	0.002	0.005	0.020	0.050	0.100
n_2 = 0.09947	-0.0359	-0.0348	-0.0301	-0.0238	-0.0176					
0.15	-0.0411	-0.0393	-0.0324	-0.0239	-0.0167					
0.2	-0.0444	-0.0421	-0.0333	-0.0234	-0.0157	-0.00408	-0.00391	-0.00322	-0.00239	-0.00167
0.25	-0.0464	-0.0435	-0.0333	-0.0227	-0.0148					
0.3	-0.0472	-0.0440	-0.0329	-0.0219	-0.0140	-0.00866	-0.00821	-0.00653	-0.00465	-0.00316
0.35	-0.0472	-0.0438	-0.0321	-0.0210	-0.0133					
0.4	-0.0465	-0.0430	-0.0311	-0.0201	-0.0126	-0.01335	-0.01256	-0.00973	-0.00675	-0.00449
0.45	-0.0451	-0.0416	-0.0299	-0.0192	-0.0120					
0.5	-0.0432	-0.0398	-0.0286	-0.0182	-0.0114	-0.01784	-0.01670	-0.01271	-0.00866	-0.00569

N_{Pr} / n	Inner Turbulent Layer: $\frac{\phi}{1 + 0.0076\, N_{Pr}\, N_{Re}^{0.9}}$					Inner Turbulent Layer: $\int_{n_2}^{0.5} \frac{\phi\, dn}{1 + 0.0304\, N_{Re} N_{Pr}^{0.9}\,(n - n^2)} + \int_{0.5}^{n} \frac{\phi\, dn}{1 + 0.0076\, N_{Pr} N_{Re}^{0.9}}$				
	0.002	0.005	0.020	0.050	0.100	0.002	0.005	0.020	0.050	0.100
0.5	-0.0432	-0.0398	-0.0286	-0.0182	-0.0114	-0.01784	-0.01670	-0.01271	-0.00866	-0.00569
0.55	-0.0408	-0.0376	-0.0069	-0.0172	-0.0107					
0.6	-0.0378	-0.0348	-0.0250	-0.0160	-0.0100	-0.02189	-0.02043	-0.01539	-0.01037	-0.00676
0.65	-0.0344	-0.0317	-0.0227	-0.0145	-0.0091					
0.7	-0.0306	-0.0282	-0.0202	-0.0129	-0.0081					
0.75	-0.0264	-0.0243	-0.0174	-0.0111	-0.0069					
0.8	-0.0217	-0.0200	-0.0144	-0.0092	-0.0057	-0.02784	-0.02592	-0.01933	-0.01289	-0.00833
0.85	-0.0167	-0.0154	-0.0111	-0.0071	-0.0044					
0.9	-0.0114	-0.0105	-0.0076	-0.0048	-0.0030					
0.95	-0.0060	-0.0055	-0.0039	-0.0025	-0.0016					
1.00	0	0	0	0	0	-0.03002	-0.02792	-0.02076	-0.01381	-0.00890

TABLE VIII

CALCULATION OF TEMPERATURE DIFFERENCES FOR N_{Re} = 100,000

For all N_{Pr} / n	Laminar Sublayer									
	$\int_0^n \phi \, dn$									
0.0005	-1.228×10^{-7}									
0.0010	-4.749×10^{-7}									
0.0015	-10.484×10^{-7}									
n_1 = 0.002087	-20.070×10^{-7}									
	Buffer Layer									
N_{Pr}	$\frac{\phi}{1 - N_{Pr} + 0.0152 N_{Pr} N_{Re}^{0.9} n}$					$\int_{n_1}^{n} \frac{\phi \, dn}{1 - N_{Pr} + 0.0152 N_{Pr} N_{Re}^{0.9} n} \times 10^{-6}$				
n	0.002	0.005	0.020	0.050	0.100	0.002	0.005	0.020	0.050	0.100
n_1 = 0.002087	-0.00184	-0.00184	-0.00184	-0.00184	-0.00184					
0.003	-0.00248	-0.00248	-0.00247	-0.00243	-0.00238	-1.97	-1.97	-1.96	-1.95	-1.93
0.004	-0.00308	-0.00307	-0.00303	-0.00245	-0.00283	-4.76	-4.75	-4.71	-4.64	-4.53
0.0049964	-0.00356	-0.00355	-0.00347	-0.00334	-0.00313	-8.08	-8.06	-7.97	-7.79	-7.51
0.007	-0.00438	-0.00435	-0.00420	-0.00394	-0.00356	-16.02	-15.95	-15.64	-15.06	-14.20
0.01	-0.00551	-0.00545	-0.00516	-0.00467	-0.00403	-30.85	-30.65	-29.68	-27.96	-25.57
n_2 = 0.01253	-0.00639	-0.00630	-0.00585	-0.00513	-0.00425	-45.91	-45.51	-43.61	-40.35	-36.03

TABLE VIII (Continued)

CALCULATION OF TEMPERATURE DIFFERENCES FOR N_{Re} = 100,000

N_{Pr} / n	Outer Turbulent Layer: $\frac{\phi}{1 - 0.0304\, N_{Pr}\, N_{Re}^{0.9}\,(n - n^2)}$					$\int_{n_2}^{n} \frac{\phi\, dn}{1 + 0.0304\, N_{Pr}\, N_{Re}^{0.9}\,(n - n^2)}$				
	0.002	0.005	0.020	0.050	0.100	0.002	0.005	0.020	0.050	0.100
n_2 = 0.01253	-0.00631	-0.00610	-0.00522	-0.00405	-0.00295					
0.05	-0.01631	-0.01449	-0.00930	-0.00542	-0.00320	-0.00046	-0.00042	-0.00028	-0.00019	-0.00012
0.1	-0.02172	-0.01778	-0.00968	-0.00478	-0.00241	-0.00141	-0.00123	-0.00076	-0.00044	-0.00027
0.15	-0.02535	-0.01957	-0.00915	-0.00443	-0.00238					
0.2	-0.02738	-0.02024	-0.00878	-0.00412	-0.00219	-0.00391	-0.00316	-0.00168	-0.00089	-0.00051
0.25	-0.02841	-0.02033	-0.00839	-0.00386	-0.00203					
0.3	-0.02875	-0.02008	-0.00801	-0.00364	-0.00191	-0.00673	-0.00518	-0.00252	-0.00128	-0.00071
0.35	-0.02863	-0.01966	-0.00766	-0.00345	-0.00180					
0.4	-0.02813	-0.01909	-0.00732	-0.00328	-0.00171	-0.00959	-0.00714	-0.00329	-0.00162	-0.00089
0.45	-0.02734	-0.01843	-0.00701	-0.00313	-0.00163					
0.5	-0.02633	-0.01771	-0.00671	-0.00300	-0.00156	-0.01232	-0.00898	-0.00399	-0.00194	-0.00106

N_{Pr} / n	Inner Turbulent Layer: $\frac{\phi}{1 + 0.0076\, N_{Pr}\, N_{Re}^{0.9}}$					$\int_{n_2}^{0.5} \frac{\phi\, dn}{1 + 0.0304\, N_{Pr} N_{Re}^{0.9}(n - n^2)} + \int_{0.5}^{n} \frac{\phi\, dn}{1 + 0.0076\, N_{Pr} N_{Re}^{0.9}}$				
	0.002	0.005	0.020	0.050	0.100	0.002	0.005	0.020	0.050	0.100
0.5	-0.02633	-0.01771	-0.00671	-0.00299	-0.00156					
0.55	-0.02501	-0.01682	-0.00638	-0.00284	-0.00148					
0.6	-0.02334	-0.01569	-0.00595	-0.00265	-0.00138	-0.01480	-0.01065	-0.00462	-0.00222	-0.00120
0.65	-0.02135	-0.01436	-0.00545	-0.00243	-0.00126					
0.7	-0.01907	-0.01283	-0.00486	-0.00217	-0.00113					
0.75	-0.01648	-0.01109	-0.00420	-0.00188	-0.00098					
0.8	-0.01365	-0.00918	-0.00348	-0.00155	-0.00081	-0.01856	-0.01318	-0.00558	-0.00265	-0.00142
0.85	-0.01054	-0.00709	-0.00269	-0.00120	-0.00062					
0.9	-0.00723	-0.00486	-0.00184	-0.00082	-0.00043					
0.95	-0.00379	-0.00255	-0.00097	-0.00043	-0.00022					
1.00	0	0	0	0	0	-0.01996	-0.01412	-0.00594	-0.00280	-0.00150

TABLE IX

CALCULATION OF TEMPERATURE DIFFERENCES FOR N_{Re} = 1,000,000

For all N_{Pr} / n	Laminar Sublayer									
	$\int_0^n \phi \, dn$									
0.00005	-1.24×10^{-9}									
0.00010	-4.88×10^{-9}									
0.00020	-19.03×10^{-9}									
n_1=0.0002628	-32.29×10^{-9}									
	Buffer Layer									
N_{Pr}	$\frac{\phi}{1 - N_{Pr} + 0.0152 N_{Pr} N_{Re}^{0.9} n} \times 10^4$					$\int_{n_1}^n \frac{\phi \, dn}{1 - N_{Pr} + 0.0152 N_{Pr} N_{Re}^{0.9} n} \times 10^8$				
n	0.002	0.005	0.020	0.050	0.100	0.002	0.005	0.020	0.050	0.100
n_1=0.0002628	-2.377	-2.377	-2.377	-2.377	-2.377					
0.0004	-3.416	-3.411	-3.385	-3.332	-3.249	-3.98	-3.98	-3.96	-3.92	-3.87
0.0005	-4.117	-4.105	-4.050	-3.945	-3.780	-7.75	-7.73	-7.68	-7.56	-7.38
0.0006290	-4.842	-4.823	-4.724	-4.538	-4.259	-17.10	-17.05	-16.83	-16.37	-15.65
0.0008	-5.799	-5.764	-5.594	-5.281	-4.831	-35.29	-35.11	-34.31	-32.76	-30.49
0.0010	-6.886	-6.829	-6.556	-6.070	-5.403		-57.97	-56.04	-52.53	-47.82
n_2=0.001577	-9.870	-9.725	-9.060	-7.969	-6.638	-83.60	-83.03	-79.54	-73.38	-65.50

TABLE IX (Continued)

CALCULATION OF TEMPERATURE DIFFERENCES FOR N_{Re} = 1,000,000

N_{Pr} / n	$\frac{\phi}{1 + 0.0304\, N_{Pr}\, N_{Re}^{0.9}\,(n - n^2)} \times 10^4$					$\int_{n_2}^{n} \frac{\phi\, dn}{1 + 0.0304\, N_{Pr}\, N_{Re}^{0.9}\,(n - n^2)}$				
	0.002	0.005	0.020	0.050	0.100	0.002	0.005	0.020	0.050	0.100
n_2=0.001577	-9.375	-9.405	-8.038	-6.232	-4.528					
0.004	-20.26	-18.55	-13.36	-8.321	-5.316					
0.01	-39.67	-33.16	-18.18	-9.568	-5.335					
0.05	-90.57	-55.61	-18.93	-8.181	-4.193	-0.000281	-0.000215	-0.000087	-0.000042	-0.000023
0.1	-103.33	-55.39	-16.04	-6.951	-3.519	-0.000774	-0.000492	-0.000176	-0.000080	-0.000043
0.15	-104.05	-52.34	-14.98	-6.184	-3.118					
0.2	-101.47	-49.23	-13.74	-6.638	-2.837	-0.001806	-0.001015	-0.000328	-0.000142	-0.000075
0.25	-97.93	-46.45	-12.77	-5.222	-2.624					
0.3	-94.09	-43.97	-11.97	-4.885	-2.453	-0.002784	-0.001482	-0.000457	-0.000195	-0.000101
0.35	-90.35	-41.81	-11.31	-4.610	-2.314					
0.4	-86.68	-39.86	-10.74	-4.374	-2.195	-0.003688	-0.001900	-0.000570	-0.000241	-0.000124
0.45	-83.14	-38.06	-10.24	-4.169	-2.102					
0.5	-79.73	-36.49	-9.81	-3.990	-2.002	-0.004520	-0.002282	-0.000673	-0.000283	-0.000145

TABLE IX (Continued)

CALCULATION OF TEMPERATURE DIFFERENCES FOR N_{Re} = 1,000,000

	Inner Turbulent Layer									
	$\frac{\phi}{1 + 0.0076\, N_{Pr} N_{Re}^{0.9}}$					$\int_{n_2}^{0.5} \frac{\phi\, dn}{1 + 0.0304\, N_{Pr} N_{Re}^{0.9}(n - n^2)} + \int_{0.5}^{n} \frac{\phi\, dn}{1 + 0.0076\, N_{Pr} N_{Re}^{0.9}}$				
N_{Pr} / n	0.002	0.005	0.020	0.050	0.100	0.002	0.005	0.020	0.050	0.100
0.5	-0.007973	-0.003643	-0.000980	-0.000398	-0.000200					
0.55	-0.007578	-0.003462	-0.000932	-0.000379	-0.000190					
0.6	-0.007075	-0.003233	-0.000870	-0.000363	-0.000178	-0.005272	-0.002626	-0.000765	-0.000321	-0.000164
0.65	-0.006477	-0.002960	-0.000797	-0.000324	-0.000163					
0.7	-0.005788	-0.002644	-0.000712	-0.000289	-0.000145					
0.75	-0.005005	-0.002287	-0.000615	-0.000250	-0.000126					
0.8	-0.004145	-0.001894	-0.000510	-0.000207	-0.000104	-0.006412	-0.003147	-0.000906	-0.000378	-0.000193
0.85	-0.003202	-0.001463	-0.000394	-0.000160	-0.000080					
0.9	-0.002196	-0.001004	-0.000271	-0.000110	-0.000055					
0.95	-0.001152	-0.000526	-0.000142	-0.000058	-0.000029					
0.1	0	0	0	0	0	-0.006838	-0.003342	-0.000958	-0.000399	-0.000203

equations (41) through (44) for various Reynolds and Prandtl moduli. Graphs of the resulting temperature distributions are shown in Figs. 12 through 15.

The computations for T are shown in Tables X through XIII. The functions in the five right-hand columns of these tables are plotted in Figs. 16 through 20. The functions were integrated graphically with a planimeter; and the results, utilizing equations (45) and (46), are shown in Table XIV.

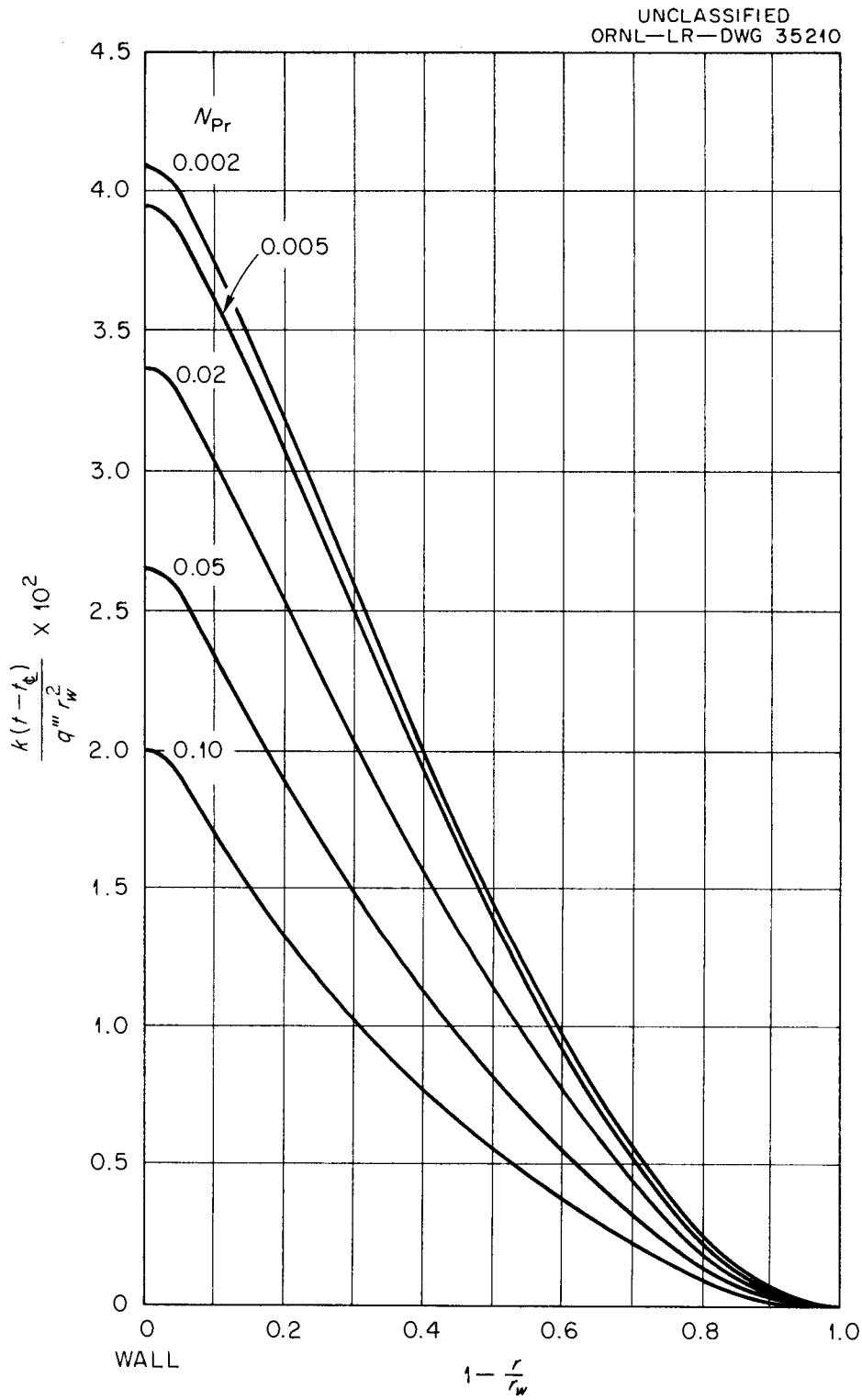

Fig. 12. Dimensionless Temperature Differences for N_{Re} = 5000 and Insulated Wall.

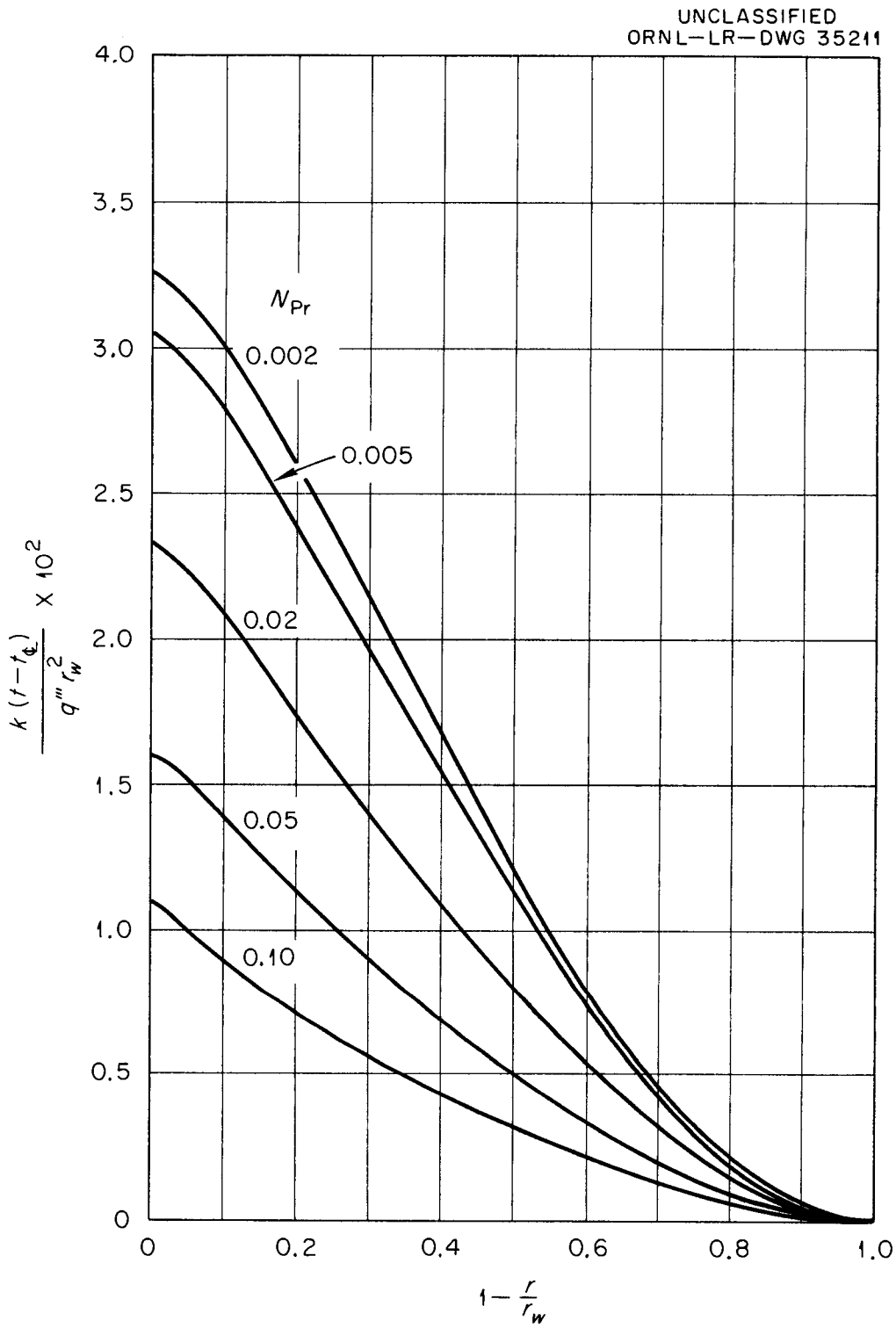

Fig. 13. Dimensionless Temperature Differences for $N_{Re} = 10,000$ and Insulated Wall.

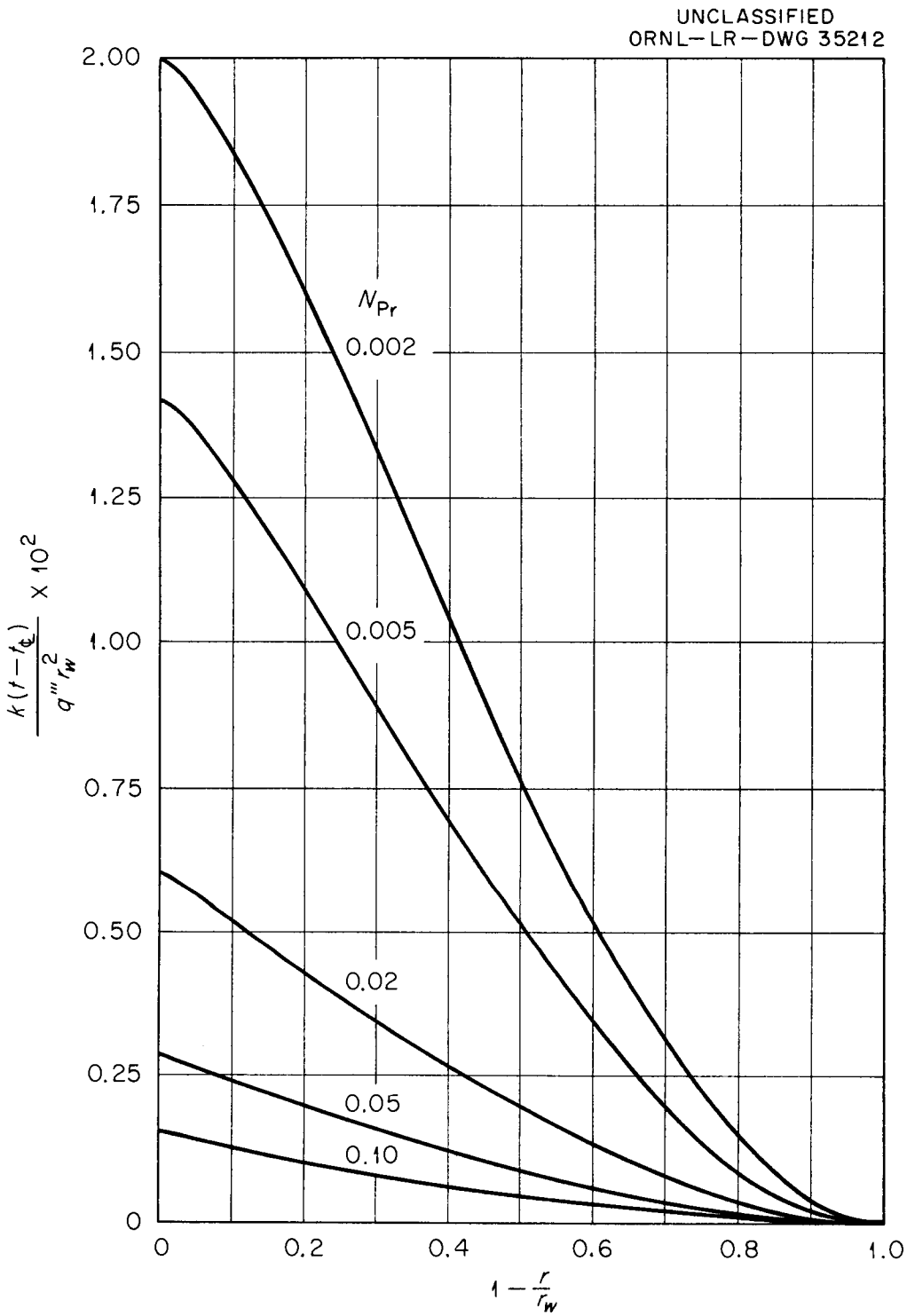

Fig. 14. Dimensionless Temperature Differences for $N_{Re} = 100,000$ and Insulated Wall.

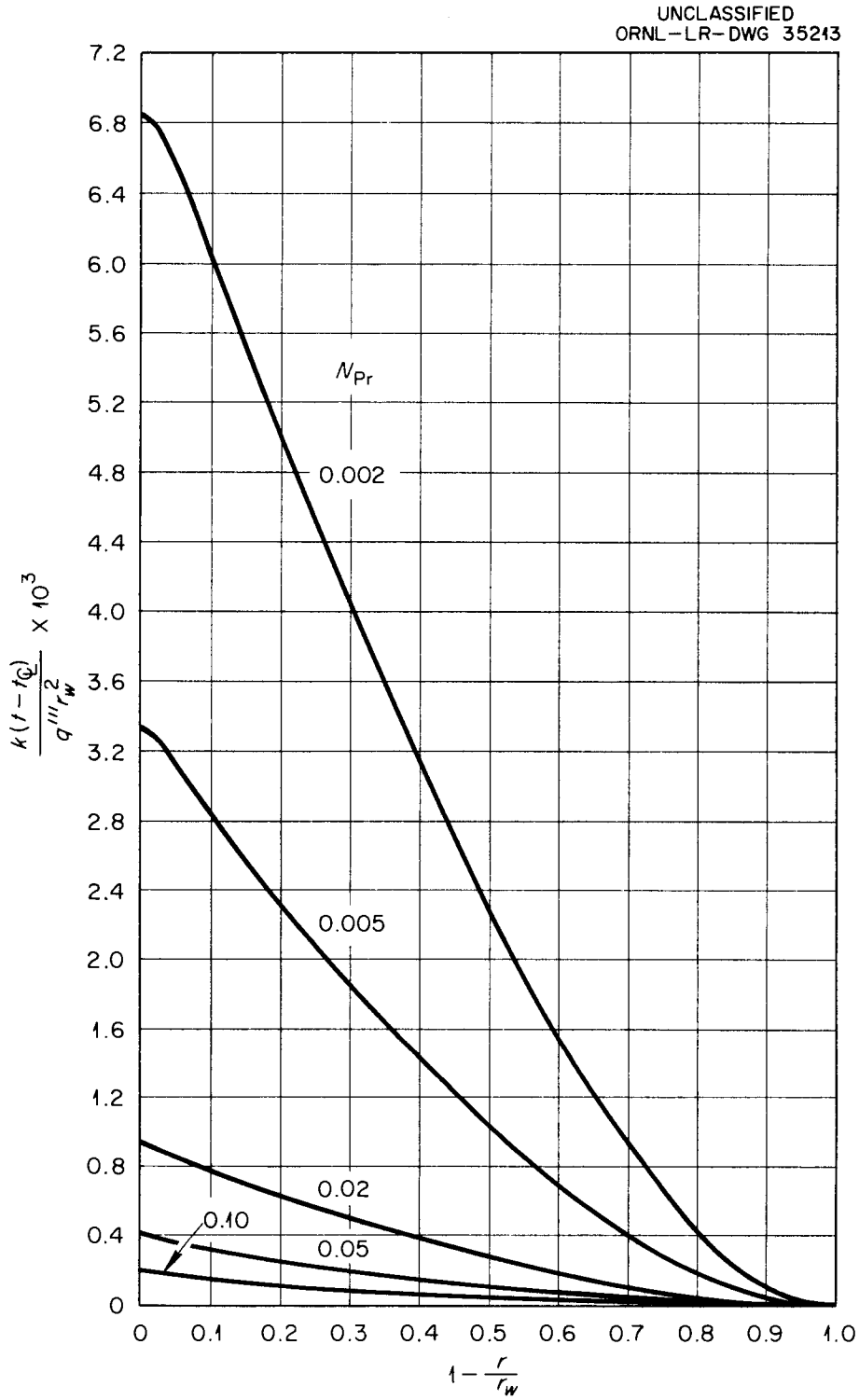

Fig. 15. Dimensionless Temperature Differences for N_{Re} = 1,000,000 and Insulated Wall.

TABLE X

CALCULATION OF T FOR N_{Re} = 5000

N_{Pr} / n	$\frac{k(t_w - t)}{q''' r_w^2}$					$S(1-S)\,0.0155\,N_{Re}^{0.8}\,\frac{k(t_w - t)}{q''' r_w^2} \times 10^5$				
	0.002	0.005	0.020	0.050	0.100	0.002	0.005	0.020	0.050	0.100
0	0	0	0	0	0	0	0	0	0	0
0.005	0.000012	0.000012	0.000012	0.000012	0.000012	0.0630	0.0630	0.0630	0.0630	0.0630
0.015	0.000107	0.000107	0.000107	0.000107	0.000107	1.656	1.656	1.656	1.656	1.656
0.025	0.000288	0.000288	0.000288	0.000288	0.000288	7.344	7.344	7.344	7.344	7.344
0.03094	0.000433	0.000433	0.000433	0.000433	0.000433	13.59	13.59	13.59	13.59	13.59
0.05	0.001050	0.001046	0.001043	0.001036	0.001025	52.20	52.00	51.84	51.50	50.98
0.06	0.001453	0.001448	0.001440	0.001424	0.001399	85.80	85.47	85.05	84.02	82.60
0.07406	0.002113	0.002103	0.002070	0.002043	0.001975	151.64	150.92	148.55	146.60	141.70

N_{Pr} / n	$\frac{k(t_w - t)}{q''' r_w^2}$					$fS(1-S)^{1/7}\,\frac{k(t_w - t)}{q''' r_w^2}$				
	0.002	0.005	0.020	0.050	0.100	0.002	0.005	0.020	0.050	0.100
0.08	0.002369	0.002358	0.002333	0.002285	0.002212	0.001956	0.001956	0.001936	0.001896	0.001836
0.11	0.003879	0.003856	0.003786	0.003655	0.003465	0.003256	0.003239	0.003180	0.003070	0.002910
0.15	0.006037	0.005996	0.005828	0.005528	0.005112	0.005060	0.005028	0.004890	0.004638	0.004285
0.30	0.014826	0.014530	0.013315	0.011548	0.009715	0.01130	0.01108	0.01016	0.008810	0.007405
0.50	0.026245	0.025466	0.022338	0.018237	0.014390	0.01537	0.01491	0.01309	0.01068	0.008432
0.60	0.031180	0.030278	0.026186	0.021051	0.016334	0.01500	0.01457	0.01260	0.01013	0.007857
0.80	0.038345	0.037121	0.031773	0.025137	0.019156	0.00961	0.00930	0.00796	0.00630	0.00480
1.00	0.040933	0.039593	0.033791	0.026613	0.020175	0	0	0	0	0

TABLE XI

CALCULATION OF T FOR N_{Re} = 10,000

n \ N_{Pr}	$\frac{k(t - t_{\ell})}{q''' r_w^2}$					$S(1 - S)^{1/7} \frac{k(t - t_{\ell})}{q''' r_w^2}$				
	0.002	0.005	0.020	0.050	0.100	0.002	0.005	0.020	0.050	0.100
0.01	0.03246	0.03035	0.02310	0.01598	0.01086	0.01665	0.01557	0.01185	0.00820	0.00557
0.03	0.03213	0.03002	0.02277	0.01566	0.01054	0.01890	0.01765	0.01338	0.00921	0.00620
0.05	0.03162	0.02951	0.02227	0.01518	0.01010	0.01959	0.01828	0.01379	0.00940	0.00625
0.08	0.03070	0.02859	0.02139	0.01437	0.00938	0.01969	0.01833	0.01371	0.00922	0.00601
0.10	0.03002	0.02792	0.02076	0.01381	0.00890	0.01945	0.01809	0.01345	0.00894	0.00576
0.20	0.02593	0.02401	0.01754	0.01142	0.00723	0.01649	0.01526	0.01115	0.00726	0.00459
0.30	0.02135	0.01971	0.01424	0.00915	0.00574	0.01258	0.01162	0.00839	0.00539	0.00338
0.50	0.01218	0.01122	0.00805	0.00514	0.00321	0.00552	0.00508	0.00364	0.00233	0.00145
0.60	0.00813	0.00749	0.00537	0.00343	0.00214	0.00302	0.00278	0.00200	0.00128	0.00080
0.80	0.00217	0.00200	0.00144	0.00092	0.00057	0.00042	0.00039	0.00028	0.00018	0.00011
1.00	0	0	0	0	0	0	0	0	0	0

TABLE XII

CALCULATION OF T FOR N_{Re} = 100,000

n \ N_{Pr}	$\frac{k(t - t_{\mathfrak{L}})}{q''' r_w^2}$					$S(1 - S)^{1/7} \frac{k(t - t_{\mathfrak{L}})}{q''' r_w^2}$				
	0.002	0.005	0.020	0.050	0.100	0.002	0.005	0.020	0.050	0.100
0.01	0.01998	0.01414	0.00595	0.00282	0.00151	0.01025	0.00725	0.00305	0.00145	0.00078
0.05	0.01950	0.01370	0.00566	0.00262	0.00138	0.01208	0.00848	0.00351	0.00162	0.00086
0.10	0.01855	0.01289	0.00518	0.00236	0.00129	0.01202	0.00835	0.00336	0.00153	0.00083
0.20	0.01605	0.01096	0.00426	0.00192	0.00100	0.01021	0.00697	0.00271	0.00122	0.00063
0.30	0.01323	0.00894	0.00342	0.00153	0.00079	0.00780	0.00527	0.00202	0.00090	0.00047
0.50	0.00764	0.00514	0.00195	0.00087	0.00044	0.00346	0.00233	0.00088	0.00039	0.00020
0.60	0.00516	0.00347	0.00132	0.00059	0.00030	0.00193	0.00129	0.00049	0.00022	0.00011
0.80	0.00140	0.00095	0.00036	0.00016	0.00008	0.00027	0.00018	0.00007	0.00003	0.00002
1.00	0	0	0	0	0	0	0	0	0	0

TABLE XIII

CALCULATION OF T FOR N_{Re} = 1,000,000

n \ N_{Pr}	$\frac{k\,(t - t_{\mathbb{C}})}{q'''\,r_w^2}$					$S\,(1 - S)^{1/7}\,\frac{k\,(t - t_{\mathbb{C}})}{q'''\,r_w^2}$				
	0.002	0.005	0.020	0.050	0.100	0.002	0.005	0.020	0.50	0.100
0.05	0.006557	0.003127	0.000871	0.000357	0.000180	0.004060	0.001935	0.000539	0.000221	0.000111
0.10	0.006064	0.002850	0.000782	0.000319	0.000161	0.003927	0.001845	0.000506	0.000207	0.000104
0.20	0.005032	0.002327	0.000630	0.000257	0.000129	0.003197	0.001479	0.000400	0.000163	0.000082
0.30	0.004054	0.001860	0.000502	0.000204	0.000102	0.002390	0.001096	0.000296	0.000120	0.000060
0.50	0.002318	0.001060	0.000285	0.000116	0.000058	0.001050	0.000480	0.000129	0.000053	0.000026
0.60	0.001566	0.000716	0.000193	0.000078	0.000039	0.000582	0.000266	0.000072	0.000029	0.000015
0.80	0.000426	0.000195	0.000053	0.000021	0.000011	0.000083	0.000038	0.000010	0.000004	0.000002
1.00	0	0	0	0	0	0	0	0	0	0

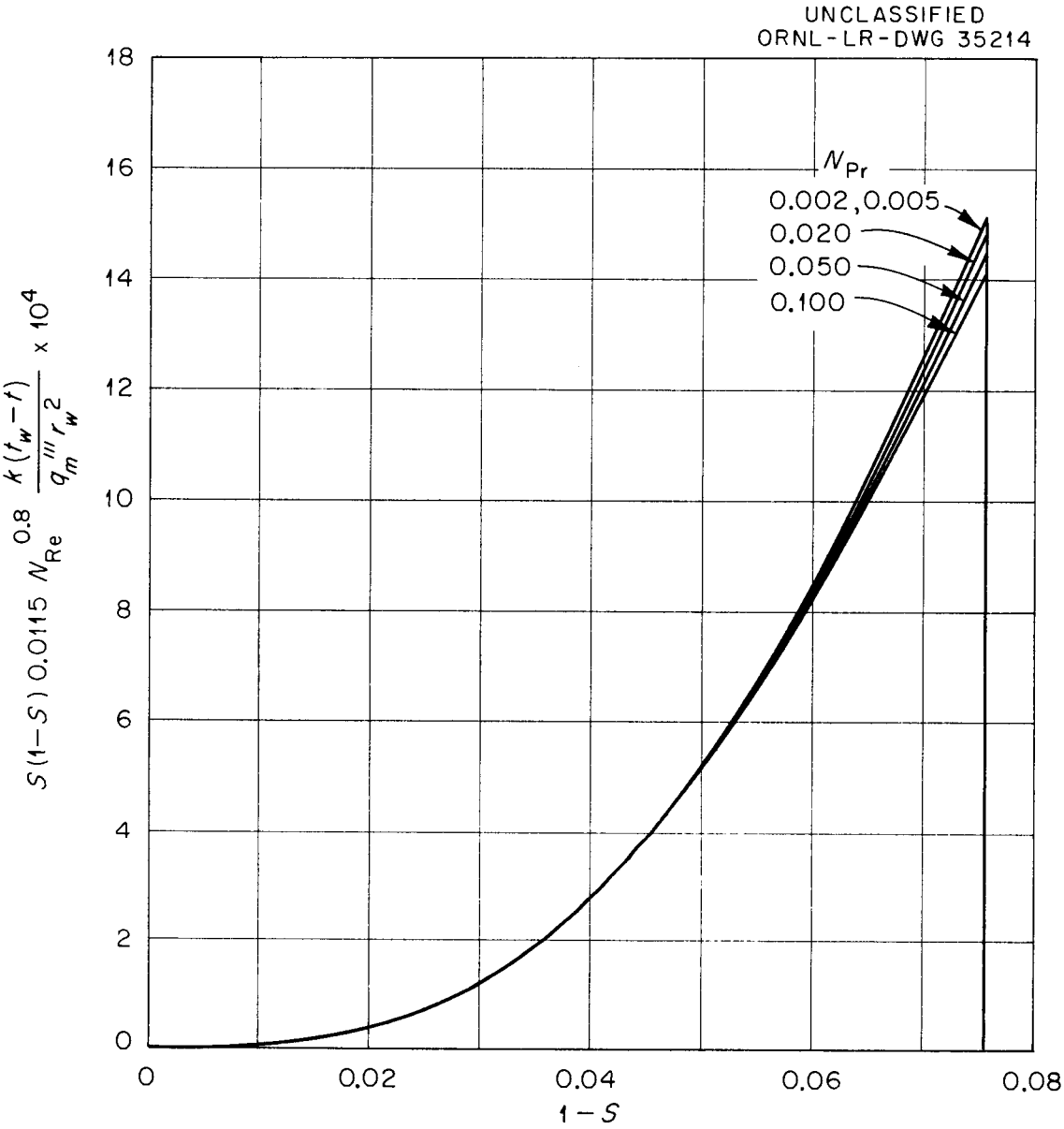

Fig. 16. Part of Integration Graph for T for $N_{Re}=5000$

$0 \leq n \leq 0.07406.$

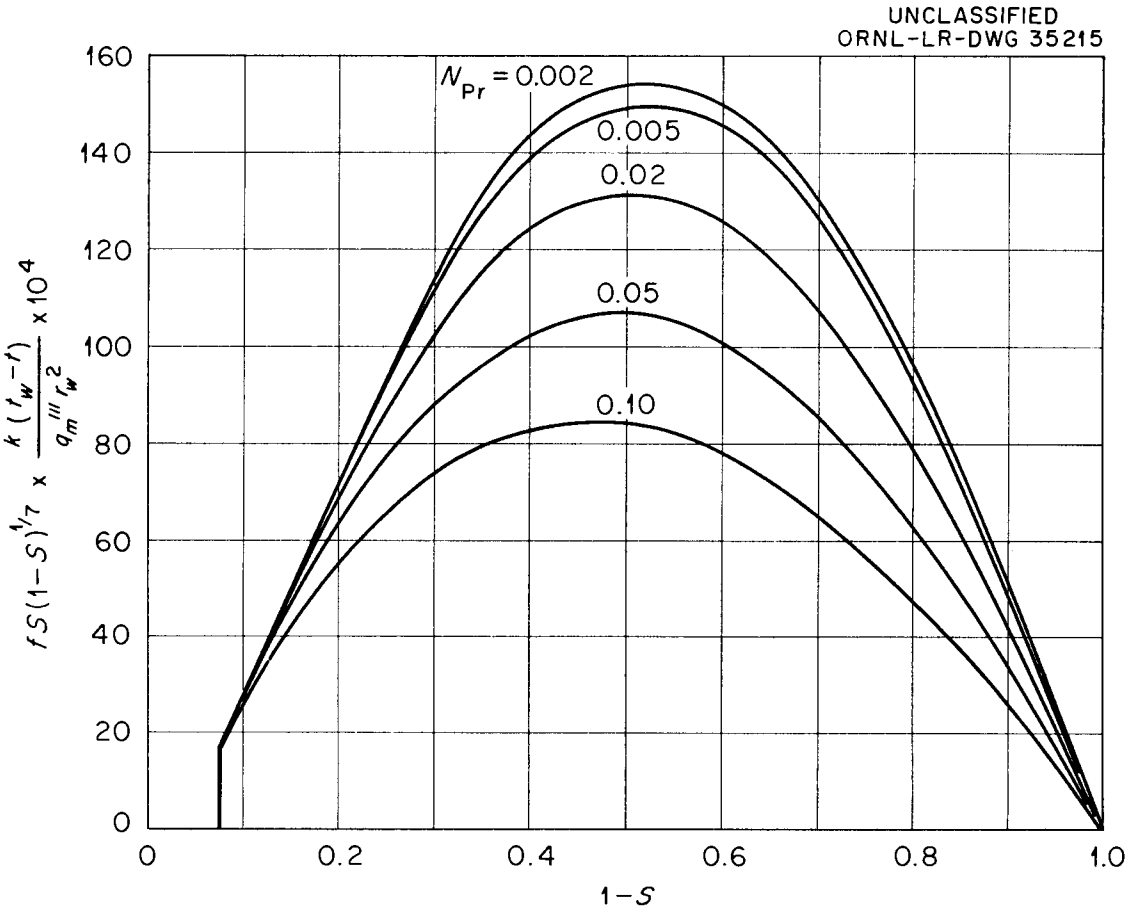

Fig. 17. Part of Integration Graph for T for $N_{Re} = 5000$
$0.07406 \leq n \leq 1.00$

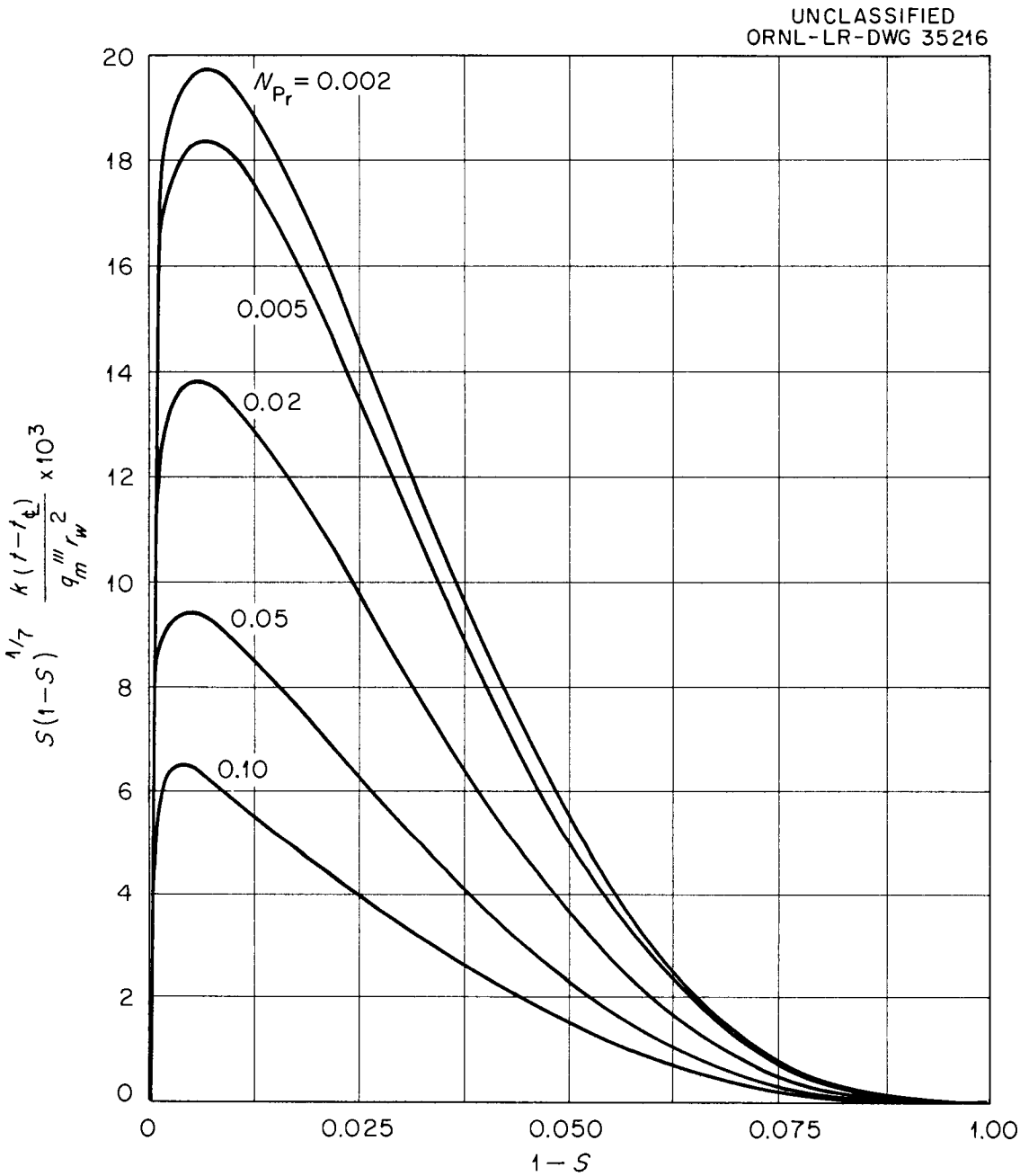

Fig. 18. Integration Graph for T for $N_{Re} = 10{,}000$.

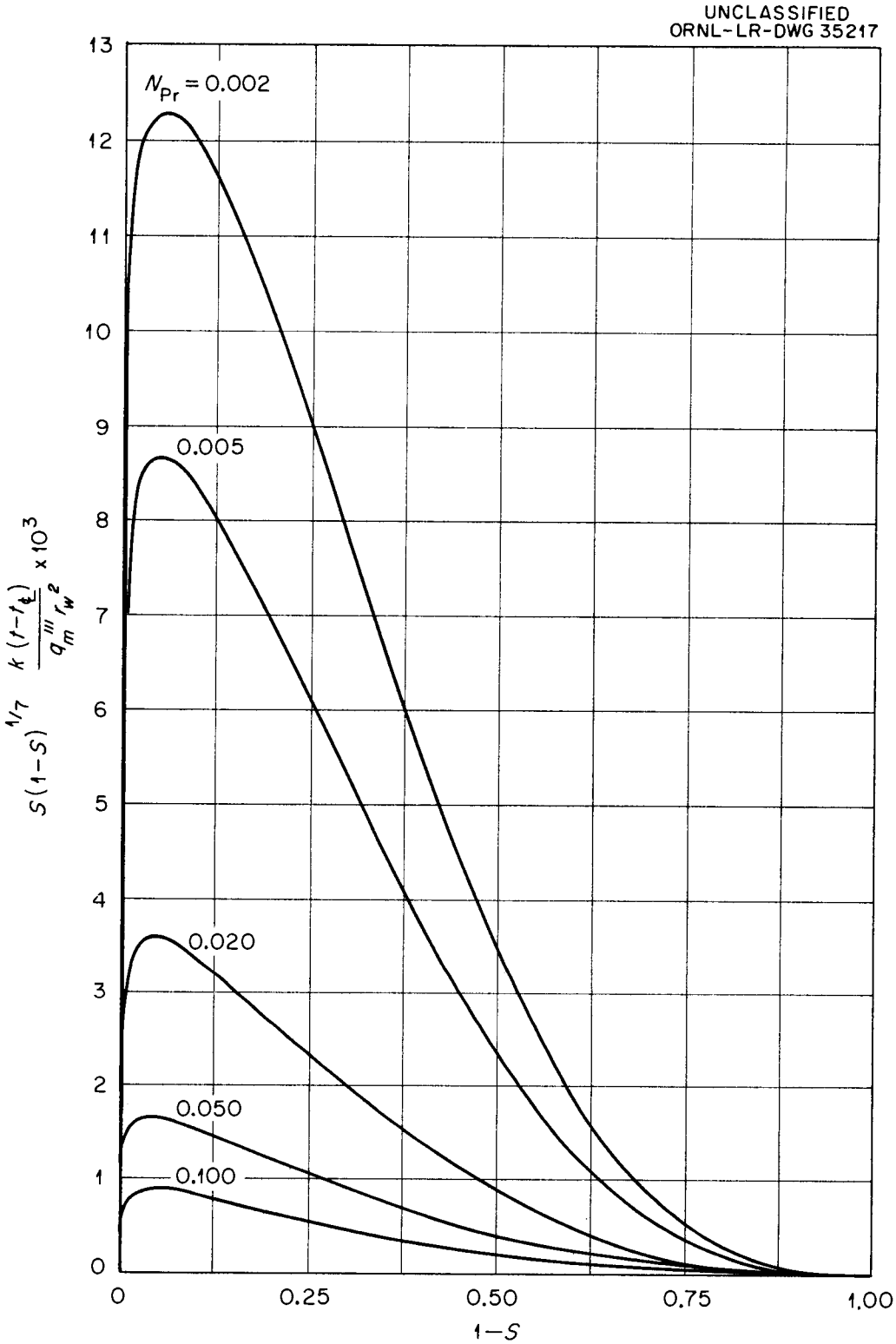

Fig. 19. Integration Graph for T for $N_{Re} = 100,000$.

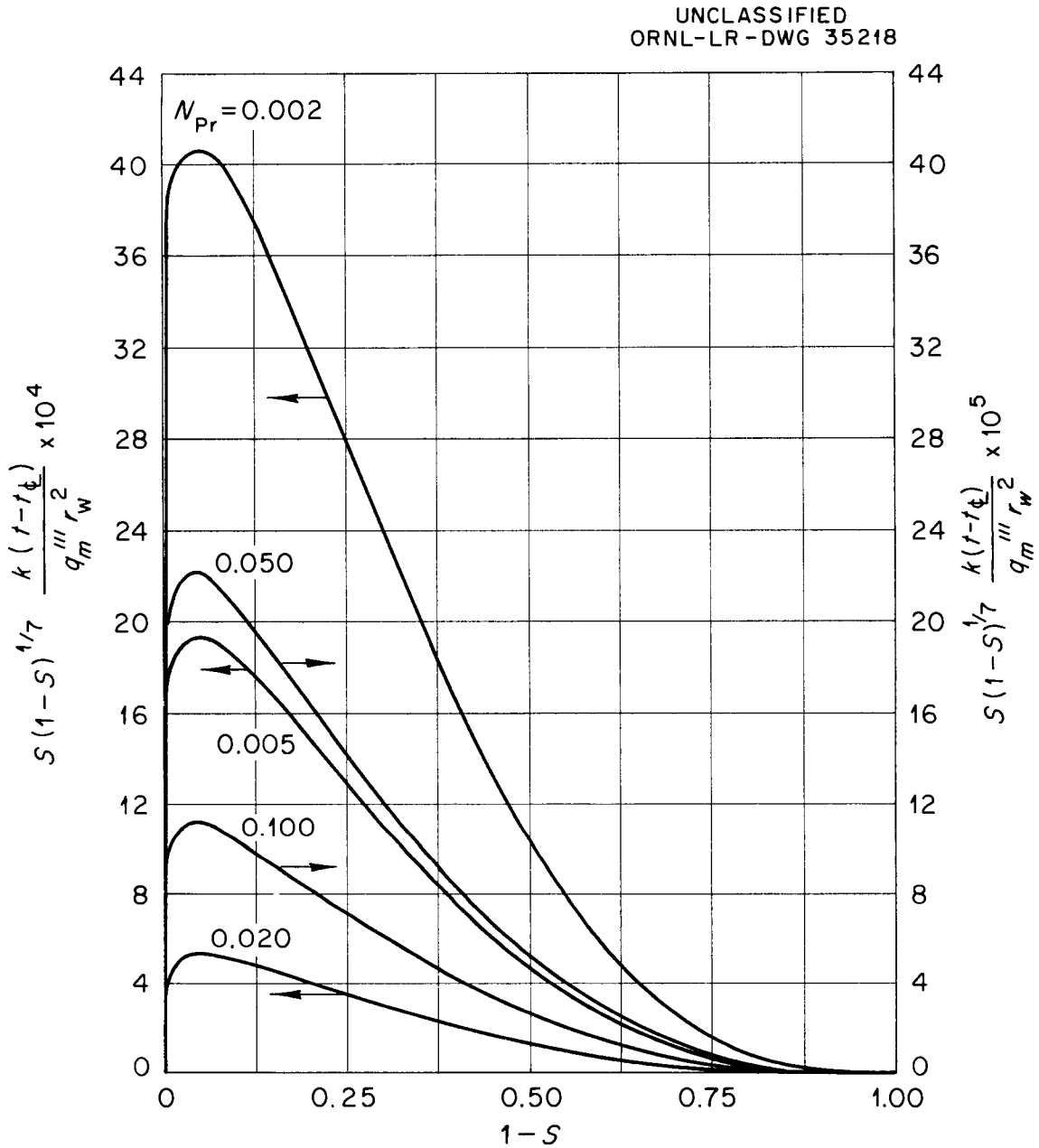

Fig. 20. Integration Graph for T for N_{Re}=1,000,000.

TABLE XIV

CALCULATION OF $k\ (t_w - t_m)/q'''\ r_w^2$ FOR VARIOUS VALUES OF REYNOLDS AND PRANDTL MODULI

N_{Pr} \ N_{Re}	$\frac{k\ (t_w - t_m)}{q'''\ r_w^2}$			
	5,000	10,000	100,000	1,000,000
0.002	0.01880	0.01400	0.008329	0.003180
0.005	0.01832	0.01317	0.006204	0.001644
0.020	0.01620	0.01053	0.002903	0.000500
0.050	0.01346	0.00776	0.001454	0.000211
0.100	0.01080	0.00558	0.000807	0.000109

B. EXPERIMENTAL RESULTS AND CALCULATIONS

The corrected experimental thermocouple measurements, orifice pressure drops, and test-section voltages and currents are tabulated in Table XV. Runs 1 through 4, 6, and 11 through 17 are the power runs. Runs 9 and 10 were made with large Δt's between the guard heaters and the test section to measure the effect of guard heater temperature on test-section wall temperatures. The resulting corrections are listed in the last column of Table XVI.

Runs 18 through 21 are thermocouple calibrations; the resulting corrections are listed in Table XVI. The raw thermocouple data were adjusted for guard heater temperature effects and corrected with this calibration data.

The calculation of the heated length was made by obtaining the resistance of each leg from the data, dividing it by the resistivity of mercury at the average leg temperature, multiplying it by the cross-sectional area. The center of the heated length was assumed to be the midplane of each leg. The volumetric heat source was then found by dividing the total heat generated in the test section by its heated volume. The fraction of total temperature rise for each leg was thus obtained. The flow rate was calculated from the heat input and the measured temperature rise.

<u>Sample Calculation: Run No. 1</u>

$t_{mi} = 79.80°F$

$t_{mo} = 184.27°F$

Mercury density at $79.80°F = 844.2\ lb/ft^3$

TABLE XV

CORRECTED EXPERIMENTAL DATA

Run No. →	1	2	3	4	6	11	12	13	14	15	16	17	Guard Heater-Tube Wall Δt 10	9
Thermocouple No.	Temperature, °F													
A-1	157.20	164.05	168.10	179.20	184.80	178.88	165.17	114.50	158.02	159.47	121.51	156.69	135.24	109.97
A-2	168.47	172.39	174.46	185.60	193.56	191.37	173.30	117.02	167.58	168.22	125.41	165.69	78.02	76.10
A-3	156.21	163.90	166.95	178.55	184.23	177.93	163.68	113.55	158.05	159.03	120.82	155.52	135.85	110.50
A-4	154.14	154.05	157.04	169.27	173.49	173.60	154.47	107.26	147.90	148.63	113.35	148.34	79.76	77.22
A-5	152.85	157.19	161.01	172.66	176.98	174.50	158.75	111.00	151.88	152.86	117.13	151.78	121.08	101.76
A-6	105.46	98.83	103.82	119.63	119.50	121.48	105.75	82.93	98.13	99.02	85.23	98.75	135.61	106.83
A-7	119.77	111.87	115.76	130.27	131.56	135.89	114.79	86.20	107.36	107.75	87.81	107.22	82.90	77.89
A-8	104.33	97.39	103.82	118.40	118.72	120.09	104.34	82.02	96.79	97.40	84.28	97.00	136.80	108.00
A-9	102.17	91.22	93.96	110.41	109.52	115.87	94.20	75.30	87.01	87.85	75.43	87.76	80.89	76.98
A-10	103.04	95.76	102.04	116.38	116.84	118.45	102.74	81.20	95.20	95.76	83.12	95.46	134.71	107.02
A-11	79.50	65.20	69.50	88.95	87.06	92.31	70.24	62.12	63.70	64.03	60.42	64.33	68.00	70.47
B-1	178.13	184.83	189.12	196.97	205.51	202.50	173.18	122.35	178.91	179.81	131.36	176.42	79.99	77.55
B-2	170.02	177.09	181.75	186.61	194.24	192.01	172.54	116.65	168.28	169.72	124.88	166.30	77.21	75.92
B-3	161.37	163.08	167.47	178.01	184.46	182.90	163.63	111.88	158.51	159.52	118.96	156.40	79.19	77.13
B-4	153.72	155.05	160.32	169.93	176.34	176.14	156.88	108.26	152.06	153.67	114.67	149.49	76.15	75.21
B-5	148.52	147.26	152.02	164.70	167.33	169.16	148.42	104.13	142.44	142.86	108.37	143.50	77.61	76.08
B-6	126.30	121.71	127.14	140.75	143.97	147.33	125.96	91.46	119.27	119.44	94.34	119.25	79.92	76.38
B-7	117.26	110.88	116.16	129.77	132.85	135.59	114.63	85.47	108.62	109.51	87.85	108.47	80.51	77.05
B-8	107.86	98.75	101.36	118.30	118.60	123.40	101.70	78.88	95.19	96.00	79.91	95.07	84.73	79.28
B-9	100.67	90.81	95.05	110.58	110.94	116.29	95.12	75.32	88.38	89.61	75.85	88.43	80.67	77.00
B-10	94.16	82.04	84.27	102.83	104.20	109.25	86.46	71.13	79.23	79.74	69.83	80.63	79.65	76.53
B-11	80.00	65.24	69.54	89.25	87.10	92.36	70.29	62.17	63.72	64.09	60.45	64 41	68.02	70.54
B-12	80.00	65.45	69.75	88.55	87.15	92.19	70.29	62.22	63.90	64.87	60.52	64.65	68.05	70.60

TABLE XV (Continued)

CORRECTED EXPERIMENTAL DATA

Run No. →	1	2	3	4	6	11	12	13	14	15	16	17	Guard Heater-Tube Wall Δt 10	9
Thermocouple No.	Temperature, °F													
B-13	179.08	187.44	189.56	198.02	206.73	203.33	184.88	123.08	181.20	183.48	132.18	177.58	77.34	76.12
B-14	161.51	165.54	169.13	178.14	184.04	182.34	163.30	111.75	158.61	161.08	118.88	156.78	79.75	77.57
B-15	146.64	146.85	149.84	167.53	167.53	168.68	149.30	104.79	144.67	146.03	109.13	142.59	75.63	70.99
B-16	128.66	123.86	126.85	143.19	145.44	147.77	126.94	91.57	120.10	120.03	94.32	119.04	80.30	77.22
B-17	106.83	98.66	102.25	117.36	118.33	122.68	101.87	78.80	95.19	95.96	79.62	94.92	81.70	77.48
B-18	93.09	81.20	84.91	102.43	102.70	109.27	87.11	71.02	79.89	80.88	69.95	81.08	79.40	76.40
B-19	184.47	192.35	195.10	202.77	212.52	205.60	189.30	125.88	186.19	188.44	135.95	180.92	68.45	70.85
Orifice No.	2	2	2	3	3	3	2	2	2	2	2	3	2	2
Orifice (in. H_2O)	100	14.5	40	3.7	1.7	4.4	148	147	60	30	30	2.7	147	147
													Guard Heater Power	
Upstream Leg Voltage (v)	3.35	2.35	2.91	4.88	4.27	5.15	4.12	2.97	3.30	2.725	2.115	4.69	30.5	25.6
Downstream Leg Voltage (v)	3.35	2.36	2.91	4.87	4.26	5.15	4.12	2.98	3.30	2.725	2.12	4.68	30.0	24.8
Upstream Leg Current (amp)	588	411	506	861	756	906	718	528	566	480	384	809	1.04	0.86
Downstream Leg Current (amp)	616	422	528	910	800	950	745	542	592	494	398	845	1.025	0.825

TABLE XVI

CORRECTIONS FOR THERMOCOUPLE READINGS

Run No. →	Calibration Corrections				Corrections for Guard Heater Temperature
	18 at 58°F	19 at 118°F	20 at 148°F	21 at 222°F	$\frac{t_o - t_w}{t_s - t_o}$
Thermocouple No.	(mv)	(mv)	(mv)	(mv)	
A-2	-0.0096	-0.0088	0.0050	0.0080	0.155
A-4	-0.0068	-0.0147	-0.0087	-0.0200	0.215
A-7	-0.0096	-0.0054	0.0183	0.0259	0.293
A-9	-0.0010	-0.0081	-0.0069	-0.0245	0.207
B-1	-0.0013	-0.0056	-0.0031	0.0042	0.202
B-2	-0.0011	-0.0029	0.0025	0.0083	0.145
B-3	0.0031	-0.0083	-0.0052	-0.0067	0.184
B-4	-0.0013	-0.0176	-0.0097	-0.0653	0.141
B-5	0.0010	-0.0143	-0.0246	-0.0497	0.202
B-6	-0.0039	0.0078	0.0056	0.0102	0.189
B-7	-0.0016	-0.0064	0.0063	0.0018	0.201
B-8	0.0011	-0.0074	-0.0111	-0.0375	0.243
B-9	0.0014	-0.0075	-0.0104	-0.0385	0.206
B-10	0.0065	-0.0178	-0.0322	-0.0830	0.190
B-13	0.0110	0.0053	0.0110	0.0034	0.152
B-14	0.0162	-0.0032	0.0045	-0.0096	0.197
B-15	0.0079	-0.0086	-0.0099	-0.0339	0.155
B-16	0.0039	0.0085	0.0106	0.0181	0.209
B-17	0.0005	-0.0029	0.0006	-0.0140	0.223
B-18	0.0042	-0.0312	-0.0482	-0.1064	0.180
B-19	-0.0018	-0.0067	0	-0.0100	

Orifice No. 2 area = 3.545×10^{-4} ft^2

$\Delta p = 100$ in. $H_2O \times \frac{62.43}{12} = 520$ lb/ft^2

$$\text{Flow rate (lb/hr)} = w = 3600\ C\ A_o \sqrt{2g\ \gamma\ \Delta p} \tag{47}$$

$$= 3600 \times 0.558 \times 3.545 \times 10^{-4} \sqrt{64.4 \times 844.2 \times 520}$$

$$= 3782 \text{ lb/hr}$$

Mercury specific heat = $c_p = 0.033$ Btu/lb-°F at 132.03°F

Mercury $N_{Pr} = 0.020$ at 132.03°F

Mercury viscosity = $\mu = 3.35$ lb/ft-hr at 132.03°F

$$\text{Heat removed} = wc_p\ \Delta t = 3782 \times 0.033\ (184.27 - 79.80) \tag{48}$$

$$= 13{,}040 \text{ Btu/hr}$$

$$\text{Heat generated} = (E_{Upst}\ I_{Upst} + E_{Dnst}\ I_{Dnst}) \times 3.413 \tag{49}$$

$$= \left[3.35\ (2.46 \times 240) + 3.36\ (2.59 \times 240)\right]\ 3.413$$

$$= 13{,}880 \text{ Btu/hr}$$

$$\text{Heat balance} = \frac{13{,}040}{13{,}880} = 0.939 \tag{50}$$

$$\text{Upstream resistance} = \frac{E_{Upst}}{I_{Upst}} = 0.00567\ \Omega \tag{51}$$

$$\text{Downstream resistance} = \frac{E_{Dnst}}{I_{Dnst}} = 0.00540\ \Omega \tag{52}$$

$$\frac{q_{f\ Dnst}}{q_{f\ Total}} = \frac{\text{avg } R_{Dnst}}{\text{avg } R_{Dnst} + \text{avg } R_{Upst}} = \frac{0.00574}{0.00574 + 0.00548} = 0.511 \tag{53}$$

$$\frac{q_{f\ Upst}}{q_{f\ Total}} = 1 - \frac{q_{f\ Dnst}}{q_{f\ Total}} = 0.489 \tag{54}$$

$$\Delta t_{Dnst} = \frac{P_{Dnst}}{P_{Total}}\ \Delta t = 0.511 \times 104.47 = 53.4°F \tag{55}$$

$$\Delta t_{Upst} = \frac{P_{Upst}}{P_{Total}}\ \Delta t = 104.47 - 53.4 = 51.07°F \tag{56}$$

$$q''' = 3.413\ \rho_e \left(\frac{I}{\pi r_w^2} \right)^2 \quad , \ \rho_e \text{ at } 133.2°F = 98.7 \times 10^{-6} \text{ ohm-cm} \tag{57}$$

$$q''' = 3.413 \times \frac{98.7 \times 10^{-6}}{2.54} \left(\frac{606}{\pi (0.125)^2} \right) \times 1728 = 3.48 \times 10^{-7} \text{ Btu/hr-ft}^3$$

k at 133.2°F = 5.46 Btu/hr-ft-°F

$$\frac{q''' \ r_w^2}{k} = \frac{3.48 \times 10^{-7} \times (0.125)^2}{5.46 \times 144} = 692°F \tag{58}$$

$$\text{avg } t_w - t_m = \frac{4.11 + 3.69 + 3.27 + 3.41 + 2.37 + 3.92}{6} = 3.46°F \tag{59}$$

$$\frac{k\ (t_w - t_m)}{q'''\ r_w^2} = \frac{3.46}{6.92 \times 10^2} = 5.00 \times 10^{-3} \tag{60}$$

The power input and measured temperature rise are used to calculate the flow rate.

$$\text{Flow rate} = w = \frac{Q}{c_p\ (t_{mo} - t_{mi})} = \frac{13{,}800}{0.033 \times 104.47} \tag{61}$$

$$= 4025 \text{ lb/hr}$$

$$N_{Re} = \frac{4w}{\pi D \mu} = \frac{4 \times 4025 \times 12}{\pi \times 0.25 \times 3.35} = 73{,}300 \tag{62}$$

$$N_{Pe} = N_{Re} \cdot N_{Pr} = 73{,}300 \times 0.020 = 1466 \tag{63}$$

Prediction was 3.9×10^{-3} for $\dfrac{k\ (t_w - t_m)}{q'''\ r_w^2}$

Ratio of observed to calculated values of T:

$$\text{Ratio} = \frac{5.00 \times 10^{-2}}{3.90 \times 10^{-2}} = 1.28 \tag{64}$$

Sample Calculation of Guard Heater Temperature Correction Factor:

Run No. 9

Temperature of A3 = 110.50°F

Temperature of B3 = 77.13°F

$$t_s - t_o = A3 - B3 = 33.37°F \tag{65}$$

$$\text{Flow rate} = w = 3600\ CA_o \sqrt{2g\ \gamma\ \Delta p} \tag{66}$$

Δp = 147 in. H_2O on orifice No. 2

$$= 147 \times \frac{62.43}{12} = 764\ lb/ft^2$$

$$w = 3600 \times 0.558 \times 3.545 \times 10^{-4} \sqrt{64.4 \times 845 \times 764}$$

$$= 4594\ lb/hr$$

μ = 3.70 lb/ft-hr at 70°F

N_{Pr} = 0.0245 at 70°F

k = 4.88 Btu/hr-ft-°F at 70°F

$$N_{Re} = \frac{4w}{\pi D \mu} = \frac{4 \times 4594 \times 12}{\pi \times 0.25 \times 3.70} = 75{,}900 \tag{67}$$

$$N_{Pe} = N_{Re} \cdot N_{Pr} = 75{,}900 \times 0.0245 = 1860 \tag{68}$$

$$h = 0.625\ \frac{k}{D}\ N_{Pe}^{0.4} = 0.625\ \frac{4.88 \times 12}{0.25} \times 23 = 2980\ Btu/hr\text{-}ft^2\text{-}°F \tag{69}$$

$$\frac{q}{A} = h\ (t_w - t_m) = 2980\ (t_w - t_m) \tag{70}$$

$$t_o - t_m = (t_o - t_w) + (t_w - t_m) \tag{71}$$

k for Pyrex glass = 0.63 Btu/hr-ft-°F

$$\frac{2k}{D_i \ln (D_o/D_i)}\ (t_o - t_w) = h\ \left[(t_o - t_m) - (t_o - t_w)\right] \tag{72}$$

Solving for $t_o - t_w$,

$$t_o - t_w = \frac{h\,(t_o - t_m)}{\dfrac{2k}{2r_w \ln (r_o/r_w)} + h} = \frac{2980\,(t_o - t_m)}{\dfrac{12 \times 2 \times 0.63}{0.25 \ln 1.5} + 2980} \tag{73}$$

$$t_o - t_w = 0.952\,(t_o - t_m)$$

For B3, $t_o - t_m = 77.13 - 70.70 = 6.43°F$

Thus, $t_o - t_w = 0.952\,(6.43) = 6.12°F$

Then, $$\frac{t_o - t_w}{t_s - t_o} = \frac{6.12}{33.37} = 0.184 \tag{74}$$

C. PROPERTIES OF MERCURY

The properties of mercury were obtained from the Liquid Metals Handbook.[14] Fig. 21 shows the Prandtl number for mercury as a function of temperature. Fig. 22 shows viscosity, thermal conductivity, specific heat, and electrical resistivity plotted versus temperature. Finally, density and coefficient of expansion are shown in Fig. 23.

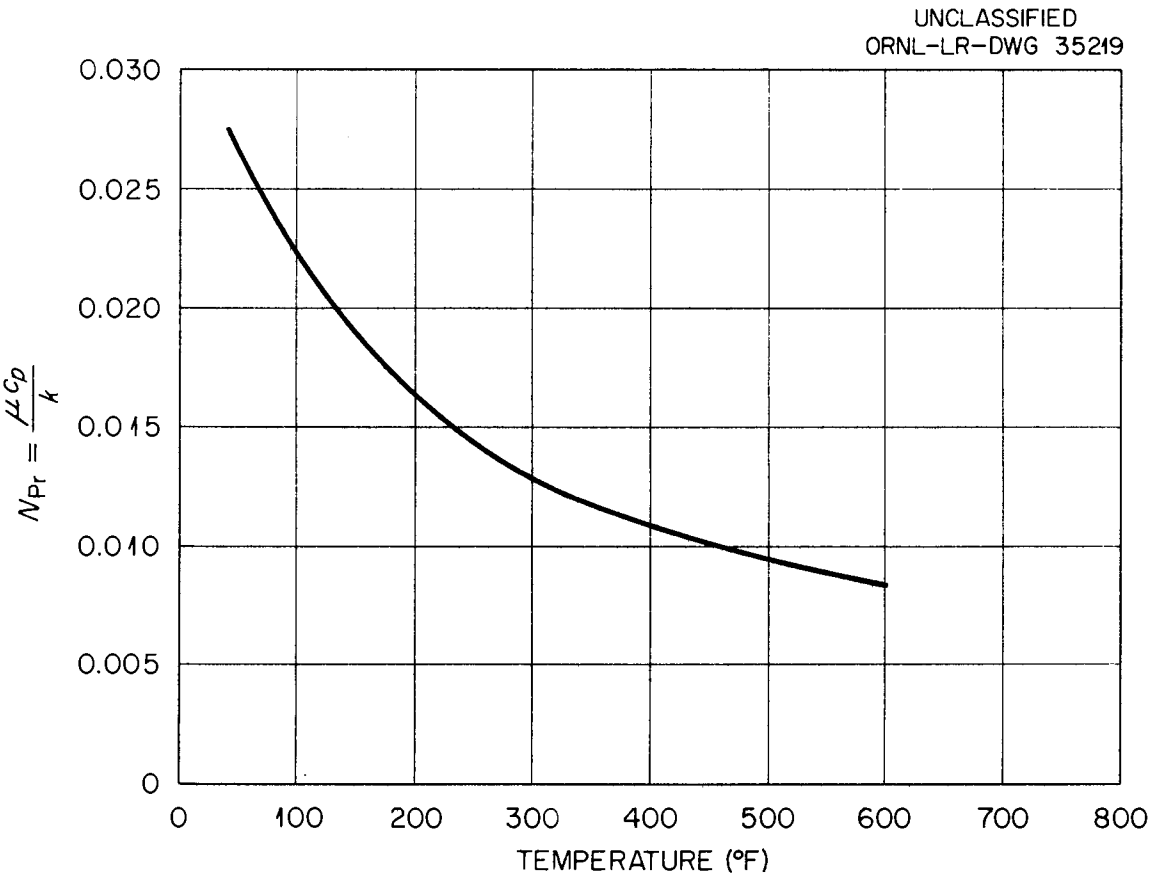

Fig. 21. Prandtl Modulus for Mercury (Reference 14)

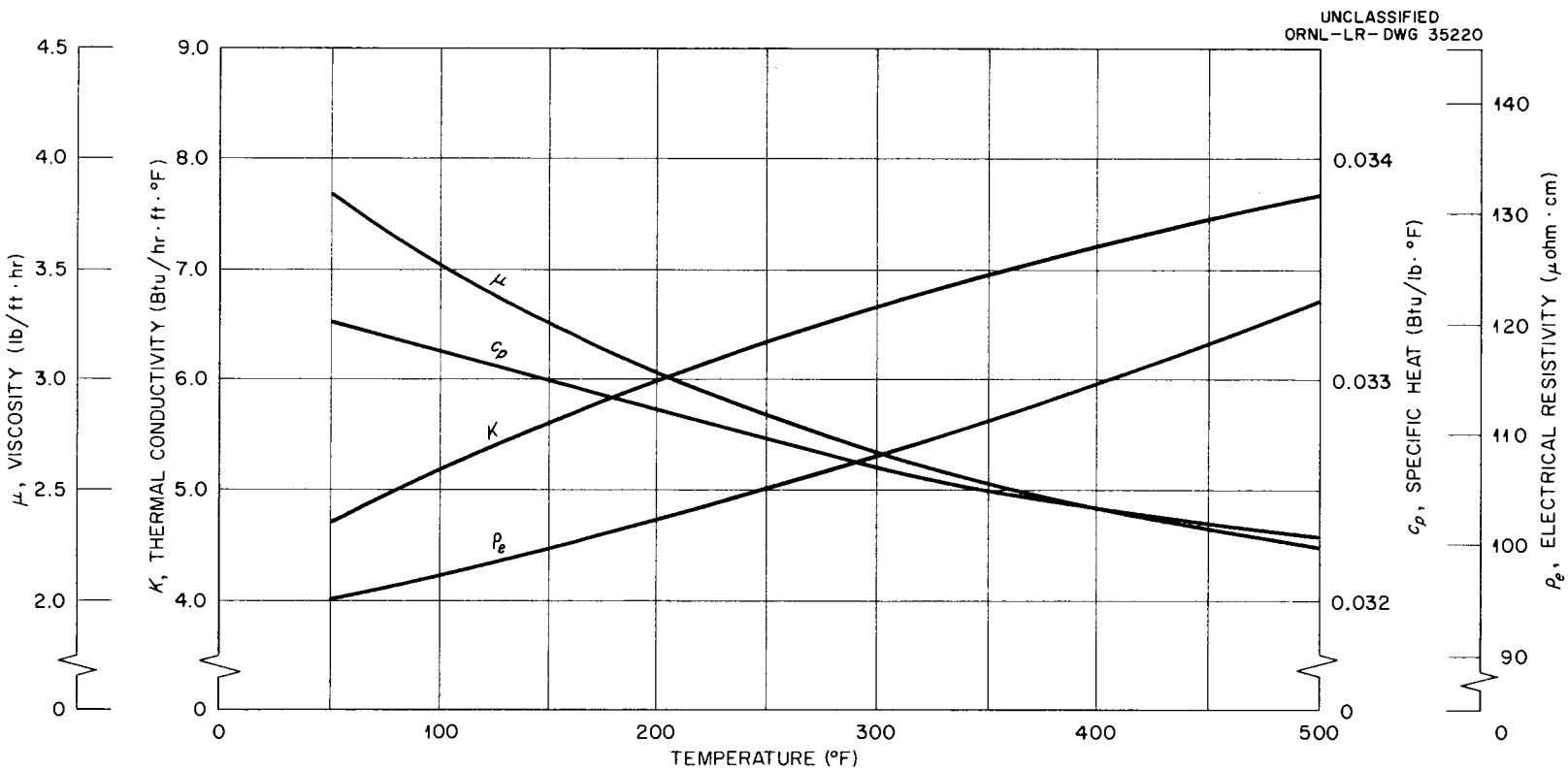

Fig. 22. Properties of Mercury – Viscosity, Thermal Conductivity, Specific Heat, Electrical Resistivity (Reference 14)

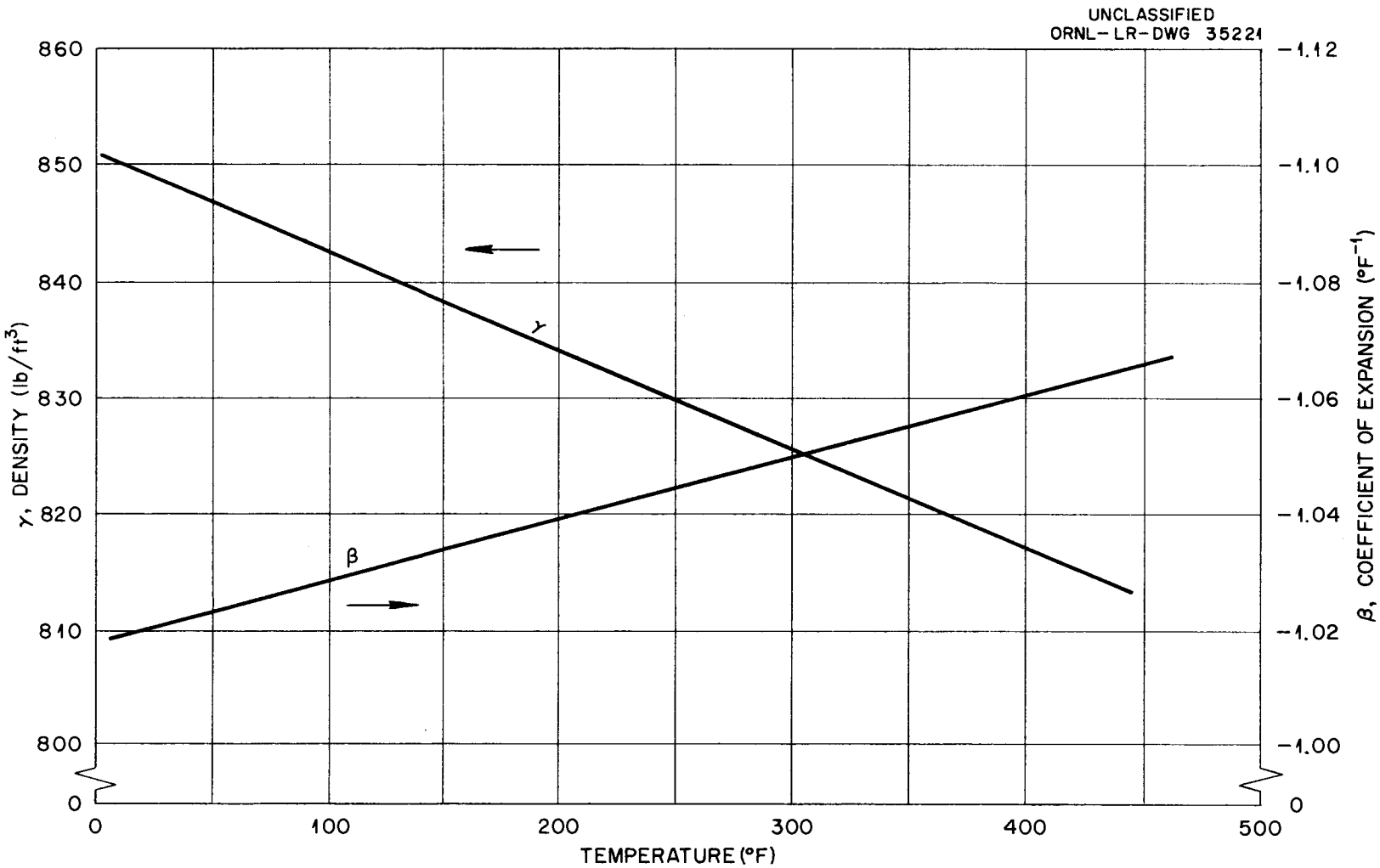

Fig. 23. Properties of Mercury – Density, Coefficient of Thermal Expansion (Reference 14)

D. LIST OF SYMBOLS

Letters

A	heat-transfer area, ft^2
A_o	orifice area, ft^2
c_p	fluid heat capacity, Btu/lb-°F
D	pipe diameter, ft
E_{Dnst}	voltage difference across downstream leg of test section, v
E_{Upst}	voltage difference across upstream leg of test section, v
g	gravitational constant, ft/sec^2
h	heat-transfer coefficient, Btu/hr-ft^2-°F
I_{Dnst}	current flow in downstream leg of test section, amp
I_{Upst}	current flow in upstream leg of test section, amp
k	fluid thermal conductivity, Btu/hr-ft^2-°F/ft
K	total thermal conductivity (molecular plus eddy), Btu/hr-ft^2-°F/ft
ℓ	length, ft
Δp	pressure difference, lb/ft^2
q_f	total internally generated heat rate in fluid, Btu/hr
q_w	wall heat flow rate, Btu/hr
q'''	volumetric heat-generation rate, Btu/hr-ft^3
q_m'''	mean volumetric heat-generation rate, Btu/hr-ft^3
r	radial distance from pipe centerline, ft
R	electrical resistance, ohm
r_w	pipe radius, ft
r_o	outside pipe radius, ft

Letters (Continued)

r_q	radius variable in heat flow integration, ft
r_t	radius variable in temperature integration, ft
t	fluid temperature, °F
$t_{\mathbb{C}}$	centerline temperature in pipe, °F
t_m	mixed-mean fluid temperature, °F
t_{mi}	test-section inlet mixed-mean temperature, °F
t_{mo}	test-section outlet mixed-mean temperature, °F
t_o	test-section outside diameter temperature, °F
t_s	insulation outside diameter or guard heater temperature, °F
t_w	wall temperature at fluid interface, °F
Δt	temperature difference, °F
u	fluid velocity, ft/hr
u_m	mean fluid velocity, ft/hr
w	flow rate, lb/hr
x	axial distance, ft
y	radial distance from pipe wall, ft
γ	fluid weight density, lb/ft^3
ϵ_h	eddy diffusivity of heat, ft^2/hr
ϵ_m	eddy diffusivity of momentum, ft^2/hr
μ	viscosity of fluid, lb/ft-hr
ν	kinematic viscosity of fluid, ft^2/hr
ρ_e	electrical resistivity of fluid, ohm-cm

Dimensionless Moduli

C = orifice coefficient

$n = 1 - \frac{r}{r_w}$

$N_{Nu} = h\, 2r_w/k$, Nusselt modulus

N_{Nu^*} = Nusselt modulus with internal heat generation in the fluid

$N_{Pr} = \mu\, c_p/k$, Prandtl modulus

$N_{Re} = u_m\, 2r_w/\nu$, Reynolds modulus

$N_{Pe} = N_{Re} \cdot N_{Pr}$, Peclet modulus

$Q''' = \frac{q'''}{q_m'''}$

$S = \frac{r}{r_w}$

$T = \frac{k\,(t_w - t_m)}{q'''\, r_w^2}$

$V = \frac{u}{u_m}$

$\alpha = \frac{\epsilon_h}{\epsilon_m}$

ORNL-2669
Physics and Mathematics
TID-4500 (14th ed.)

INTERNAL DISTRIBUTION

1. D. S. Billington
2. F. F. Blankenship
3. E. P. Blizard
4. A. L. Boch
5. C. J. Borkowski
6. G. E. Boyd
7. E. J. Breeding
8. R. B. Briggs
9. C. E. Center (K-25)
10. R. A. Charpie
11. J. W. Cooke
12. F. L. Culler
13. L. B. Emlet (K-25)
14. D. E. Ferguson
15. A. P. Fraas
16. J. H. Frye, Jr.
17. W. R. Grimes
18. E. Guth
19. C. S. Harrill
20-44. H. W. Hoffman
45. A. Hollaender
46. A. S. Householder
47. W. H. Jordan
48. G. W. Keilholtz
49. C. P. Keim
50. M. T. Kelley
51. J. J. Keyes, Jr.
52. G. J. Kidd, Jr.
53. A. I. Krakoviak
54. J. A. Lane
55. R. S. Livingston
56. F. E. Lynch
57. R. N. Lyon
58. H. G. MacPherson
59. W. D. Manly
60. J. R. McNally
61. K. Z. Morgan
62. J. P. Murray (Y-12)
63. M. L. Nelson
64. R. H. Nimmo
65. C. A. Preskitt
66. A. M. Perry
67. P. M. Reyling
68. H. W. Savage
69. A. W. Savolainen
70. H. E. Seagren
71. E. D. Shipley
72. M. J. Skinner
73. A. H. Snell
74. W. J. Stelzman
75. J. A. Swartout
76. E. H. Taylor
77. J. L. Wantland
78. A. M. Weinberg
79. C. E. Winters
80. Biology Library
81. Health Physics Library
82. Reactor Experimental Engineering Library
83-84. Central Research Library
85-104. Laboratory Records Department
105. Laboratory Records, ORNL, R. C.
106-107. ORNL Y-12 Technical Library Document Reference Section

EXTERNAL DISTRIBUTION

108. Division of Research and Development, AEC, ORO
109. Pratt and Whitney Aircraft Division (G. L. Muller)
110-724. Given distribution as shown in TID-4500 (14th ed.) under Physics and Mathematics category (75 copies - OTS)